



HAL
open science

Electrical Properties of Vertical Dominant Charge Structures Observed in Corsican Thunderstorms With a LMA

Ronan Houel, Eric Defer, Dominique Lambert, Serge Prieur, Stéphane Pédeboy

► **To cite this version:**

Ronan Houel, Eric Defer, Dominique Lambert, Serge Prieur, Stéphane Pédeboy. Electrical Properties of Vertical Dominant Charge Structures Observed in Corsican Thunderstorms With a LMA. *Earth and Space Science*, 2024, 11 (2), 10.1029/2023ea003354 . hal-04450277

HAL Id: hal-04450277

<https://hal.science/hal-04450277>

Submitted on 10 Feb 2024

HAL is a multi-disciplinary open access archive for the deposit and dissemination of scientific research documents, whether they are published or not. The documents may come from teaching and research institutions in France or abroad, or from public or private research centers.

L'archive ouverte pluridisciplinaire **HAL**, est destinée au dépôt et à la diffusion de documents scientifiques de niveau recherche, publiés ou non, émanant des établissements d'enseignement et de recherche français ou étrangers, des laboratoires publics ou privés.

Earth and Space Science



RESEARCH ARTICLE

10.1029/2023EA003354

Key Points:

- Vertical charge structures of Corsican thunderstorms and their lightning characteristics are documented based on VHF and LF observations
- 25% of storms 10 min-periods showed negative dipole structures with some of them the highest flash rates recorded during the 5-month period
- Flash polarity provided by the LF lightning locating system is consistent with the inferred charge structure

Correspondence to:

R. Houel,
ronan.houel@meteo.fr

Citation:

Houel, R., Defer, E., Lambert, D., Prieur, S., & Pédeboy, S. (2024). Electrical properties of vertical dominant charge structures observed in Corsican thunderstorms with a LMA. *Earth and Space Science*, 11, e2023EA003354. <https://doi.org/10.1029/2023EA003354>

Received 15 OCT 2023

Accepted 8 DEC 2023

Author Contributions:

Conceptualization: Ronan Houel, Eric Defer

Data curation: Serge Prieur, Stéphane Pédeboy

Formal analysis: Ronan Houel

Methodology: Ronan Houel

Resources: Stéphane Pédeboy

Software: Serge Prieur

Supervision: Eric Defer

Validation: Ronan Houel

Visualization: Ronan Houel

Writing – original draft: Ronan Houel

Writing – review & editing: Eric Defer, Dominique Lambert, Serge Prieur, Stéphane Pédeboy

Electrical Properties of Vertical Dominant Charge Structures Observed in Corsican Thunderstorms With a LMA

Ronan Houel¹ , Eric Defer¹, Dominique Lambert¹ , Serge Prieur¹, and Stéphane Pédeboy²

¹LAERO, Université de Toulouse, CNRS, UPS, IRD, Toulouse, France, ²Météorage, Pau, France

Abstract Lightning characteristics of Corsican storms with different charge structures are investigated in this study. Observations of an LMA network are used to document the total lightning activity. Complementary lightning observations of the lightning detection network Météorage are also used. A clustering algorithm is used to build a database of electrical cells from June to October 2018. A method is also applied to infer the vertical charge structure, as dominant dipoles, per 10-min period for each electrical cell. As an example, one cell recorded in July 2018 is discussed. The cell database is then presented as well as the main electrical properties according to the dominant charge structures. For instance, the higher in altitude the dominant dipole, the higher the flash rate. Overall, dominant negative dipole are observed for 25% of the 10-min periods and can be separated into two categories: (a) low altitude negative dipole class dominated by negative cloud-to-ground (CG) flashes with a main positive layer located between 2 and 4 km height and (b) high altitude negative dipole class, dominated by negative intracloud (IC) with a main positive layer at 5 km height. Dominant positive dipole can also be separated into two categories with (a) a dominant positive dipole located between 4.5 and 10 km high, –CG dominance, weak flash rate and (b) higher altitude dominant positive dipole, +IC dominance and a larger +CG fraction. The synergistic use of LMA and Météorage observations independently gives a rational type and polarity classification with regard to the vertical charge structure.

Plain Language Summary Lightning characteristics of Corsican storms with different charge layers distributions are investigated in this study. Observations of the 3D lightning imager SAETTA, deployed in Corsica, are used to document the total lightning activity. Complementary lightning observations recorded by the French operational lightning detection network Météorage are also used. An algorithm is applied on the lightning data to build a database of electrical cells from June to October 2018. A method is also applied to infer the dominant dipole charge structure per 10-min period for each electrical cell. The results show that the higher in altitude the dominant dipole, the higher the flash rate. Overall, dominant negative dipole are observed for 25% of the 10-min periods and can be separated into two categories with low and high altitude of the dominant dipole that are associated with weak and strong flash rate. The synergistic use of the 3D lightning imager and the French operational lightning detection network gives a rational type and polarity classification to observed flashes with regard to the vertical charge structure.

1. Introduction

Lightning flash rate is directly linked to vertical air motions (Deierling et al., 2008; E. R. Williams, 1985) as updrafts tend to enhance charge separation (Saunders et al., 1991). Well-organized thunderstorms with strong updrafts have larger lightning flash rates compared to ordinary storms and are generally associated with the occurrence of severe weather (e.g., Deierling et al., 2008; Gatlin & Goodman, 2010; Goodman et al., 1988; MacGorman et al., 1989; Wiens et al., 2005, and others). The tracking of the lightning activity and its properties, like the abrupt increase of the flash rate also called “lightning jump”, can be used operationally to monitor the storm intensity (Schultz et al., 2009).

Object-based tracking methods using radar reflectivity, like TITAN (Thunderstorm Identification, Tracking, Analysis and Nowcasting, Dixon & Wiener, 1993) and THOR (THunderstorm observation by Radar, Houston et al., 2015), are commonly used for monitoring individual thunderstorm cells. More recently, tracking methods using lightning-based observations have been developed. For instance Li-TRAM algorithm (Meyer et al., 2013) using observations from the European VLF/LF lightning detection network LINET (Betz et al., 2007, 2009) show that a tracking with lightning data as an independent source gives comparable results to a purely radar-based tracking but remains less efficient than a tracking using a hybrid method mixing radar and lightning data. This

© 2024 The Authors. Earth and Space Science published by Wiley Periodicals LLC on behalf of American Geophysical Union.

This is an open access article under the terms of the [Creative Commons Attribution License](https://creativecommons.org/licenses/by/4.0/), which permits use, distribution and reproduction in any medium, provided the original work is properly cited.

result suggests that lightning-based tracking algorithm alone or in addition to the radar-based tracking can be used to monitor thunderstorms.

Rebounding collisions between different ice hydrometeors cause a transfer of electrical charges according to the non inductive charging mechanism. Laboratory studies have found that depending on the temperature and on the liquid water content (LWC), graupel particles acquire charges of different polarity when colliding with ice crystals in the presence of supercooled liquid water (e.g., Jayaratne et al., 1983; Saunders et al., 1991; Takahashi, 1978). Graupel tends to charge positively (negatively) in a high (low) temperature and large (small) LWC environment while ice crystals charge negatively (positively) (e.g., Pereyra et al., 2000; Saunders & Peck, 1998). This charge transfer occurs mainly in the mixed-phase region, generally located in the cloud region between -10°C and -40°C (MacGorman & Rust, 1998). Gravitational sedimentation and differential advection of charged hydrometeors lead to net charged layers in the thundercloud (e.g., Bruning & Macgorman, 2013; E. R. Williams, 1985).

The main charge layers observed near the periphery of the updraft, where most charge separation occurs, are used to classify thunderstorm charge structures (e.g., Bruning et al., 2010). Most thunderstorms possess a normal tripole charge structure, characterized by a layer of net negative polarity at midlevels (approximately -10°C to -30°C) situated between two regions of net positive polarity. The upper positive charge layer is considered to be the most active in terms of lightning activity propagating through (Lang & Rutledge, 2011; E. R. Williams, 1989) meanwhile the lower positive charge layer is not always present (López et al., 2019; Pawar & Kamra, 2004; E. R. Williams, 1989). Normal charge structures tend to produce large fraction of negative cloud-to-ground (CG) flashes (E. R. Williams, 1989).

In comparison to normal charge structures, anomalous charge structures are characterized by a dominant layer of positive charges at the bottom of the clouds or at the same altitude range of the midlevel negative layer of the normal charge structure (e.g., Bruning et al., 2014; MacGorman et al., 2005; Rust et al., 2005; E. Williams et al., 2005). In fact, the distribution of charges of a tripole can vary vertically leading to top-heavy (normal charge structure) or bottom-heavy tripole (anomalous charge structure) structure depending on the relative activity of positive layers (e.g., Mansell et al., 2010). Since normal polarity storms have a dominant upper positive charge regions around -40°C , Fuchs et al. (2015) discussed anomalous storms as storms with a dominant positive layer at temperatures warmer than -30°C . Medina et al. (2021) define periods of storms as anomalous when the dominant positive layer altitude is below the altitude of the dominant negative layer. These bulk distributions of charge are more likely to be observed in the updrafts but more charge layers and more complicated vertical charge distributions can be observed in supercells or mesoscale convective system (MacGorman et al., 2005; Rust et al., 2005; Stolzenburg et al., 1998).

Additionally, anomalous charge structures have been found to produce significant lightning flash rates (Fuchs et al., 2015) and severe weather (Lang & Rutledge, 2011), with predominantly positive CG flashes (Carey & Buffalo, 2007; Lang et al., 2004; Lang & Rutledge, 2011; Tessendorf et al., 2007; Wiens et al., 2005). Indeed, instead of being located at the upper part of the cloud, the main positive charge layer is located at the middle or lower level, which facilitates the positive leaders to propagate to the ground and even more easily if a layer of negative charges is present between the main positive charge layer and the ground. Nonetheless, some of these anomalous storms exhibit low flash rates and no positive CG flash predominance. Anomalous charge structures have been observed in the US (Chmielewski et al., 2018; Fuchs et al., 2015, 2016, 2018; Lang et al., 2004; MacGorman et al., 2008; Rust et al., 2005; Stough & Carey, 2020; Stough et al., 2021; Tessendorf et al., 2007; Wiens et al., 2005), in Spain (Pineda et al., 2016; Salvador et al., 2021) or in Argentina (Lang et al., 2020; Medina et al., 2021).

In the absence of widespread availability of total lightning (CG and intracloud (IC) flashes) observations, the majority of the initial studies on the charge structure of thunderstorm were undertaken using CG lightning data. Anomalous charge structures were commonly linked to a high +CG production. The use of +CG production as a proxy has made it possible to identify regions with different PPCG (Predominantly Positive Cloud-to-Ground) storms in the USA without being able to quantify the frequency of occurrence of anomalous storms. More recently, new techniques have been developed to infer charge layers and detect anomalous charge structures (e.g., Fuchs et al., 2015; Medina et al., 2021; Stough & Carey, 2020). Medina et al. (2021) found that 13.3% of thunderstorms in a region of Argentina were defined by an anomalous charge structure while 82.6% of Colorado thunderstorms were anomalous, consistent with previous high PPCG storms documented in the same region.

Stough et al. (2021) analyzed the flash production of four supercells, two with a normal charge structure and two with an anomalous charge structure. Higher peak rates, +CG fraction and IC-CG ratio were associated with the anomalous supercells. This is consistent with the findings of Qie et al. (2005) and Tessendorf et al. (2007) that have reported that the presence of excessive lower positive charge prevented the occurrence of -CG flashes and favored the production of IC flashes between the two low-altitude layers. Negative CG flashes lower negative charges to the ground while +CGs lower positive charges to the ground (Bruning et al., 2014). Intracloud flash polarity follows the same convention, the sign of the charges lowered to the charge layer below is assigned to the flash. Consequently IC flashes occurring between an upper positive (negative) layer and a lower negative (positive) layer with a negative leader moving upward (downward) transports positive (negative) charges toward the lower layer and are classified as +IC (-IC) (Bruning et al., 2014). For a thundercloud with a dominant positive (negative) dipole, the IC activity of normal (anomalous) charge structures are supposed to be dominated by +ICs (-ICs) (Medina et al., 2021).

Recently, Coquillat et al. (2022) reported storms with anomalous charge structures and low flash rates in a south-western flow in Corsica region. Corsica is a large island with the highest mountains in the western Mediterranean basin and is subject to intense meteorological events such as heavy precipitation, lightning and wind storms (Lambert et al., 2011). Documenting the electrical charge structure of storms in a maritime and mountainous region such as Corsica is original and interesting for a better understanding of the spatial and temporal variability of the storm charge structure. This leads to the goal of the present study that aims at analyzing the different charge structures and the properties of the flashes observed in this region. Concurrent LMA (Lightning Mapping Array) VHF and Météorage LF observations are then used to document the total lightning activity. The lightning observations are ingested in a cell tracking algorithm designed to identify and track storms at the cell scale. Charge structures are eventually inferred for each cell using an automatic charge layer retrieval algorithm. Finally the characteristics of the lightning flashes and lightning activity are derived at the cell scale.

The paper is organized as follows: Section 2 describes the instrumentation, the area of study, the data processing, the cell tracking algorithm and the charge layer retrieval algorithm. Section 3 discusses the results successively through a case study and a statistical analysis while Section 4 summarizes the main results of the study.

2. Data and Methodology

2.1. SAETTA Lightning Mapping Array (LMA) and Study Domain

The SAETTA network (Coquillat et al., 2019) is composed of 12 Lightning Mapping Array (LMA) stations (Rison et al., 1999) deployed in Corsica Island under the PCOA (Plateforme CORSiCA d'Observations Atmosphériques) framework. Each station detects the very high frequency (VHF) radiation (60–66 MHz) emitted by both IC and CG flashes. SAETTA is able to detect the lightning activity up to approximately 350 km from the center of the network. The domain of the present study ranges from 7.5°E to 10.6°E in longitude, and from 41°N to 43.5°N in latitude. The domain of interest is centered on Corsica with a maximum north-south (or east-west) distance of 150 km from the center of the LMA network which is a reasonable range for a good retrieval accuracy of the VHF source altitude and consequently a good estimate of the altitude of the charge structures (Chmielewski & Bruning, 2016; Dotzek et al., 2004; Thomas et al., 2004).

2.2. French Total Lightning Detection Network (Météorage)

The French operational Lightning Locating System Météorage (MET) consists in 21 LF (Low Frequency) Vaisala LS7002 sensors distributed over France and was, in 2018, a contributor to the European Cooperation for Lightning Detection (EUCLID; Schulz et al., 2016). Météorage locates CG strokes as well as IC pulses. The polarity of CG strokes is determined by the sign of charge transported to ground. ICs pulses associated to a transport of negative charge downward are labeled -ICs and those transporting positive charge downward are labeled +ICs (Cummins & Murphy, 2009; Leal et al., 2019).

Météorage is the operator of a Low Frequency (LF) Lightning Locating System (LLS) which covers the Western Europe based on the most recent Vaisala technology, namely LS7002 sensors coupled with a Total Lightning Processor (TLP). In 2018, Météorage was a member of EUCLID, a European Cooperation for Lightning Detection (Shultz et al., 2016). The system is made of about 90 sensors owned by Météorage complemented with sensors

belonging to partnering neighboring national LLS operators which detect the electromagnetic signals associated with the large vertical charge transfers occurring between opposite charge centers in the cloud and between the cloud and the ground, producing return strokes and intra-cloud pulses. The lightning data set analyzed in this study was mainly observed by the 12 closest sensors located in a maximum range of 350 km from Corsica.

Pédeboy et al. (2018) reported a detection efficiency of 97% and 56% for CG flashes and IC flashes, respectively. Cloud-to-ground stroke location accuracy is about 150 m (Pédeboy, 2015) while the median IC location accuracy is about 1.64 km (Pédeboy et al., 2018).

As the MET network works similarly to the U.S NLDN (National Lightning Detection network) (e.g., Cummins et al., 1998; Orville, 2008), we will rely on the tests performed with NLDN to reclassify some MET observations. Indeed, it has been shown that NLDN strokes with currents below +10 kA are probably IC pulses misclassified and that IC pulses with currents above +20 kA are in fact CG strokes (Biagi et al., 2007; Cummins & Murphy, 2009). The population of records with current between +10 and +20 kA is a mixture of CG strokes and IC pulses. The NLDN has been upgraded and the IC-to-CG and CG-to-IC swaps are no longer required (Murphy et al., 2021) but as the Météorage network was not yet upgraded in 2018, we use the same thresholds as in Fuchs et al. (2015) and Pineda et al. (2016): all positive (negative) IC pulses with a current $> +25$ kA (< -25 kA) are reclassified as CG strokes with the same polarity and current. In addition, all positive (negative) CG strokes with currents $< +10$ kA (> -10 kA) are reclassified as IC pulses. The reclassification of IC pulses and CG strokes induces for the 5 months of study an increase of 6% of the number of IC pulses and a decrease of almost the same percentage in the number of CG strokes.

2.3. L2b Data, LMA Flash Classification and Period of Study

SAETTA raw data (L0) are combined together to derive locations and times of VHF sources, that is, L1 SAETTA data (Rison et al., 1999; Thomas et al., 2004). The L2 SAETTA data consist in VHF sources merged together to form flashes. A Python scikit-learn package DBSCAN (Density-Based Spatial Clustering of Applications with Noise) algorithm (Pedregosa et al., 2011) is used to pair VHF sources based on a combination of temporal and spatial criteria, similarly to Fuchs et al. (2016) or Ma et al. (2021).

The L2b data consist in MET CG strokes and IC pulses merged to SAETTA L2 flash data. Indeed to take advantage of the synergy of both VHF and LF observations, MET stroke/pulse records are combined to SAETTA L2 flashes based on temporal and spatial criteria. Both spatial and temporal pairings are performed incrementally using successively finer settings. This incremental procedure translates into a quality parameter that qualifies the merging between the LF and VHF records and that can be used as data filter. First a LF stroke/pulse belongs to a given VHF flash when (a) the absolute time difference between that specific LF event and any VHF source that composes that flash is below 200 ms, and (b) its location is within a 0.4° -latitude 0.4° -longitude box centered at the location of any VHF source. If this first check is validated, the temporal and spatial pairing is then refined by applying successively a finer time window (20 ms, and then 2 ms) and a 2D distance criteria (5 km for a CG stroke; 10 km for a IC pulse). This multiple-step process aims at limiting the computation time during the pairing and at including potentially mis-located lightning records. The LF event is eventually paired to the flash that contains the closest VHF source in time and space. Each MET stroke/pulse finally possesses, in addition to time, latitude, longitude, peak current, and event type (IC or CG), three new attributes: the VHF flash number to which it belongs, the VHF source number to which it has been paired, and a pairing quality factor (not detailed here).

The merging of MET and SAETTA records allows classifying SAETTA flash as CG (+CG, -CG), IC (+IC, -IC and Dual IC), "LMA only" and ambiguous (flashes with dual polarity CG strokes). Dual IC flashes correspond to 15% of the total number of flashes in the study database (27% of the flashes in the IC category) while ambiguous flashes represent only 1% of the total flash population. Dual IC and ambiguous flashes are discarded of this analysis since no unique polarity could be assigned to them. A flash is qualified as +CG (-CG) flash if it contains at least one positive (negative) MET CG stroke and only positive (negative) MET CG strokes no matter the number and the polarity of the MET IC pulses paired to that same flash. A CG flash being the extension toward the ground of an IC flash (e.g., Bruning et al., 2014) it is likely to find some MET IC pulses in the first microseconds of a CG flash and later as well. So, a vast majority of CG flashes has both MET IC pulses and MET strokes associated. A flash is qualified as IC if it has at least one MET IC pulse and only MET IC pulses. It then can be classified as +IC or -IC if all the MET IC pulses associated to that flash exhibit the same polarity.

Otherwise the flash is classified as dual IC flash. The reclassification of IC pulses and CG strokes mentioned in Section 2.2 mainly leads to a decrease in the number of -CG flashes in favor of -IC flashes. Any flash is then depicted by a list of VHF sources and potentially by a series of CG strokes and/or IC pulses. Different flash properties are then determined like the flash duration or the flash initiation height. Two methods have been tested to determine the flash initiation height: the first method basically used the altitude of the first VHF source of each flash as initiation height while the second method computes the mean altitude of the VHF sources in the first 500 μs of each flash. A study on 3,500 flashes revealed that the standard deviation of the altitude difference between these two methods was around 70 m. The second method was finally used since it reduces the impact of outliers on flash initiation height calculation.

In order to remove the number of noisy sources, only VHF sources detected by a minimum of 7 stations and with a reduced-chi square lower than 0.5 are kept similarly to Coquillat et al. (2019). In addition, flashes with less than 10 VHF sources are also filtered out (e.g., Mecikalski et al., 2017; Salvador et al., 2021; Schultz et al., 2015; Wiens et al., 2005). About 84.2% of the flashes recorded during the study period are filtered out with 93.6% (93.5%) of them having a flash duration lower than 1 ms (100 μs). The study period ranges from the beginning of June to the end of October 2018 (JJASO 2018). It encompasses the Enhanced Observation Period (EOP) of the EXAEDRE (EXploiting new Atmospheric Electricity Data for Research and the Environment; <https://www.hymex.org/exaedre/?page=home>) project, during which specific cloud and rain measurements were conducted at the EXAEDRE supersite in Corsica.

2.4. Electrical Cell Tracking Algorithm (ECTA)

The goal of this study is to investigate the electrical activity at the storm scale during its lifetime. For this reason one needs to identify and track the storm cells during their entire life cycle. As the study only uses electrical data, the thunderstorm cells are called electrical cells. We define an electric cell as adjacent L2b flashes clustered in time and space, cluster that moves with time. The clustering uses a 2D flash density, also called Flash Extent Density (FED), computed from all individual L2b flashes time-stamped during 5 min and computed on a regular grid of 1 km^2 pixels. Flash Extent Density clusters are computed within each given 5-min period by an application of two successive DBSCAN (Pedregosa et al., 2011) methods applied on the pixels. The algorithm ECTA is presented in further details in Appendix A. The algorithm allows to build a database of electrical cells. Each electrical cell is then described by all corresponding L2b data. Several electrical properties such as the flash rate, the percentage of each type of flash, the flash initiation along the life of the cell are then deduced. All electrical cells lasting less than 20 min and composed of less than 20 L2b flashes are filtered out as the study focuses on typical cells in the Mediterranean region (Galanaki et al., 2018) with a sufficient lifetime and electrical activity. The excluded short-lived cells correspond to weak lightning activity or are related to artifacts due to misidentified electrical cells from the cell tracking algorithm, isolated flashes or discontinuous extended flashes separated in multiple clusters, or electrical cells entering or outgoing the geographical domain.

2.5. Charge Layer Identification and Samples Definition

As mentioned in Section 1, the purpose of this study is to characterize the electrical properties at the scale of the thunderstorm cell. It has been shown that the charge structure in thunderstorms is directly related to the electrical activity (Bruning et al., 2014; Fuchs et al., 2018; Tessoro et al., 2007; Wiens et al., 2005). The charge structure of the cells is studied here by adapting the *Chargepol* algorithm (Medina et al., 2021) applied on the LMA VHF sources. This algorithm aims at deducing coarse polarity layers from a flash-by-flash analysis. It is based on the bilevel intracloud discharge model (Kasemir, 1960; Mazur & Ruhnke, 1993; Van Der Velde & Montanyà, 2013) where a flash initiates between two charge layers of opposite polarity.

By principle, the algorithm can only detect, for each flash, the presence of two charge layers that form a dipole in which the flash propagated. A more complex structure (e.g., tripole) cannot be deduced with a single flash even if the flash propagates in all layers. However an agglomeration of several flashes, cumulated over the time and clearly qualified by *Chargepol* algorithm, still provides some insights on the charge structure with potentially several representation of charge layers retrieved at different altitudes. Moreover, this reduces the impact of occasional *Chargepol* algorithm errors on the determination of the charge layers.

The *Chargepol* algorithm was applied to the flashes with the same conditions (e.g., minimum 20 VHF sources per flash) on the flashes as in Medina et al. (2021). One additional condition has been added on the total duration of the flash, which had to be greater than the preliminary breakdown duration (i.e., 10 ms). Indeed we found some rare flashes with a duration of less than 10 ms, that were qualified by *Chargepol* algorithm but which then exhibited no VHF sources after the 10 ms period. From the entire 5-month database of electrical cells, 98,948 (31%) of the 292,513 flashes with at least 10 VHF sources were qualified by the *Chargepol* algorithm.

Figure 1a shows an example of the application of *Chargepol* algorithm on the flashes of a cell extracted from the database (cell #2 from the 26 July 2018, see appendix A). Out of a total of 287 flashes, 139 (48.4%) were qualified by *Chargepol* algorithm of which 114 were identified as +ICs flashes and 25 as -ICs flashes, the polarity being defined by the propagation direction of the initial negative leader. Note that the flash classification as +IC or -IC flash provided by *Chargepol* algorithm is not used at all in the present study. Figure 1b reveals a coarse tripolar

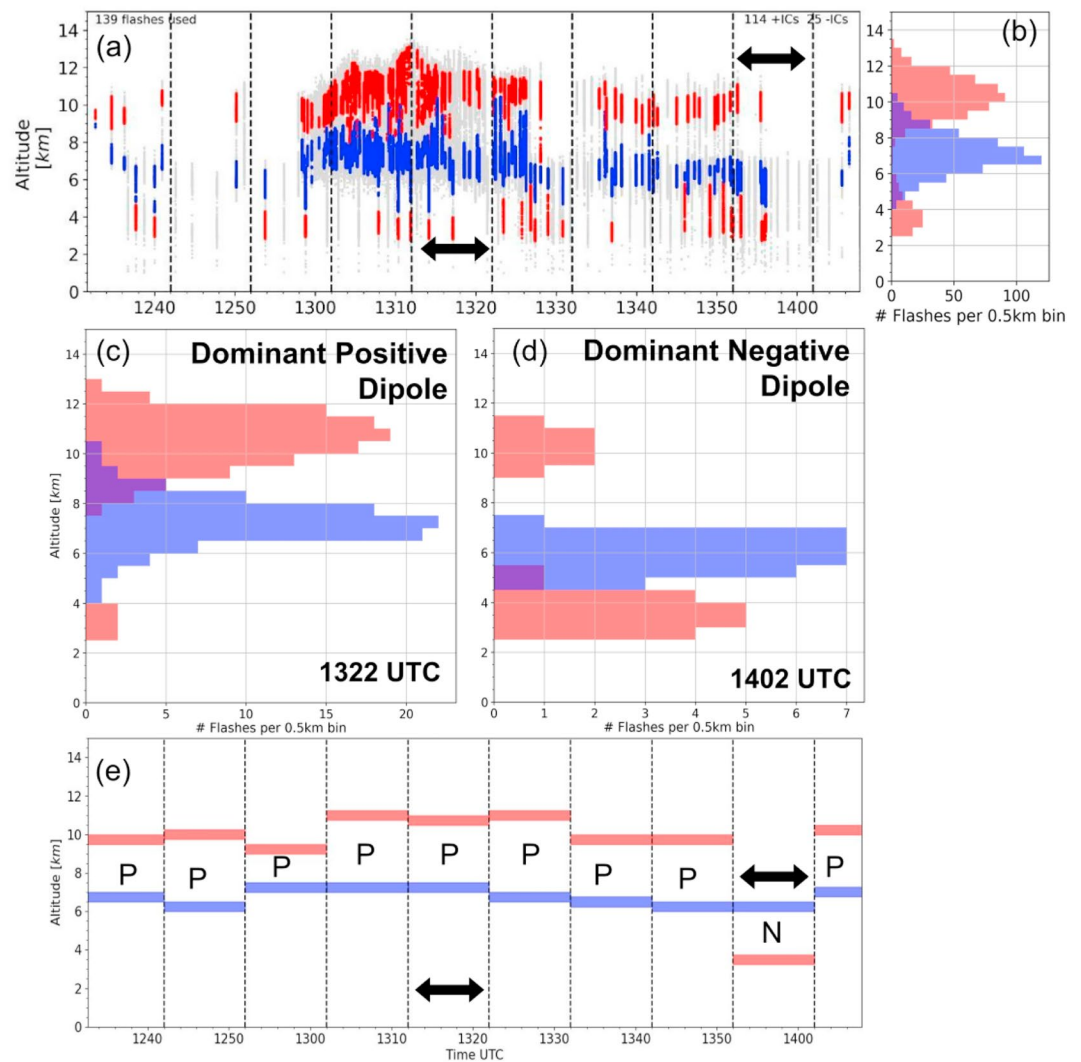


Figure 1. Charge layers inferred from *Chargepol* algorithm at cell-scale. (a) Altitude of VHF sources versus time for the cell #2 on the 26 July 2018. VHF sources in an inferred positive (negative) charge layer are colored in red (blue). VHF sources with no polarity inferred are colored in gray. Each vertical black dashed line represents the end of a sample and the start of a new one. (b) Histogram (0.5 km bins) over the vertical of *Chargepol*-flashes propagating in an identified positive or negative charge layer for the cell #2. (b) and (c) show histograms (0.5 km bins) of vertical distribution of *Chargepol*-flashes propagating in inferred positive and negative charge layers altitude for the 1322 UTC and 1402 UTC samples (black arrows in (a) and (e), time associated to the end of the samples). (e) Altitude of samples DPL (red) and DNL (blue) versus time for cell #2. Each vertical black dashed line represents the end of a sample and the start of a new one. “P” for dominant Positive dipole samples, “N” for dominant Negative dipole samples.

structure at the scale of the electrical cell as deduced from the agglomeration of *Chargepol*-flashes (flashes qualified by the *Chargepol* algorithm). Overall, the electrical cell exhibits a lower positive layer between 2 and 5 km, a main negative midlevel layer between 5 and 8 km and an upper positive layer between 8 and 13 km (Figure 1b). Looking at the modes of the vertical distribution of the *Chargepol*-flashes (Figure 1b), the dominant positive layer is located at the upper part of the thundercloud with a maximum of 95 identified 0.5-km-bin flashes propagating in an identified positive charge layer between 10 and 10.5 km height. A secondary positive charge layer mode with a maximum of 25 identified 0.5-km-bin flashes propagating in an identified positive charge layer is found between 3 and 4 km. This cell thus exhibits a normal tripolar charge structure (E. R. Williams, 1989) with a more pronounced upper positive layer inducing a dominant activity in the positive dipole located in the upper part of the cloud during a large part of the cell life cycle.

A charge structure can evolve during the life of an electrical cell and can show a wide range of possible charge layer stacks depending on the storm life-cycle (dissipation phase, mature phase or storm oscillation process; Pawar & Kamara, 2007). For this reason, it is difficult to assign the same charge structure to an entire cell that can potentially exhibit a continuum of charge structures (Bruning et al., 2010). On the other hand, one can separate a cell into successive short periods and identify the predominant charge structures. Medina et al. (2021) use 1-hr periods, called samples, to analyze their LMA observations. In the present study, 10-min periods, also called samples, are used as the median life duration of the Corsican electrical cells is 58 min, and visual inspection of the vertical distribution of the lightning activity and consequently the vertical structure of the charge regions can evolve significantly within an hour. The goal is to qualify the dominant dipole for each 10-min sample by automatically identifying the altitude of the dominant positive layer (DPL) and the altitude of the dominant negative layer (DNL). A sample is in fact composed of a succession of flashes (all the flashes of the 10-min period) and is labeled thanks to its dominant charge structure. Each flash, when qualified by *Chargepol* algorithm, provides an image of both positive and negative charge layers in which its branches propagate through. For each given sample, the distribution of the altitude of the *Chargepol*-flashes is computed per 0.5 km altitude bin by counting the number of *Chargepol*-flashes with at least one VHF source associated with a positive or negative charge layer detection.

As in Medina et al. (2021), the DPL and DNL altitude for each sample are identified from the altitudes modes of the *Chargepol*-flashes propagating in positive and negative inferred charge layers. Figure 1c (1d) shows an example of the *Chargepol*-flashes distribution over the altitude for a dominant positive dipole (dominant negative dipole) sample. In case of equality between mode values of a given polarity, the average of the mode altitudes is then computed. However, each sample must have a standard deviation of the altitude of the *Chargepol*-flashes vertical distribution modes lower than 2 km. It is designed to filter out samples with dominant layers exhibiting equal altitude mode amplitudes. Since the charge layers observed in Corsica are generally less than 4 km thick, this criterion eliminates the cases where perfectly balanced tripoles structures do not allow the methodology to designate a dominant dipole.

In addition, one needs to assure that for any sample both DPL and DNL correspond well to the predominant charge structure of the entire sample and not only of the few flashes analyzed by *Chargepol*. This verification is performed by filtering the samples based on the confidence of the charge layer retrieval by *Chargepol*. Medina et al. (2021) filtered out 1-hr samples with a maximum value of the *Chargepol*-flashes vertical distribution lower than 30 flashes of both polarities to mitigate the influence of low flash rate storms on charge layers estimation. In the present study, a similar filtering could be applied with a minimum of 5 *Chargepol*-flashes per 10 min-period to be consistent with Medina et al. (2021) but such filter cannot be applied here since almost 50% of the samples exhibits less than 5 flashes qualified by *Chargepol* algorithm.

In consequence a multi-parameter filter has been designed. Indeed the samples kept for the study must have a minimum of one *Chargepol*-flash and a ratio between the number of *Chargepol*-flashes and the total number of flashes of the sample greater than or equal to 0.2. We notice that samples with few flashes are generally associated to relatively high confidence ratio by nature. Finally, DPL and DNL heights must be at different altitudes. Samples with DPLs above DNLs are classified as dominant positive dipole samples while samples with DNLs above DPLs can be classified as dominant negative dipole samples.

Figure 1e reveals that all samples in cell #2 except the one finishing at 1402 UTC (Figure 1d) are associated with a dominant positive dipole (positive over negative). The dominant positive (negative) layer reached a maximum altitude of 10.5 km (7 km) during the mature phase of the storm in association probably with the intensification

Table 1

Number of Samples and Flashes Statistics Before and After Filtering on Samples for Each Month Independently and for the 5 Months Together

	June 2018	July 2018	August 2018	September 2018	October 2018	Total (JJASO 2018)
# Cells obtained with ECTA	98	77	229	118	189	711
# Raw samples	769	577	1666	931	1399	5,342
Dominant Positive/Negative/Unknown dipole for raw samples (%)	56/31/13	74/21/5	82/12/6	73/18/9	44/42/14	66/24/10
# Total Flashes	18,166	37,410	88,781	41,905	106,251	292,513
<i>Chargepol</i> flashes (% of total flashes)	44	34	34	30	26	31
# Filtered samples (% of raw samples)	587 (76%)	482 (83%)	1375 (83%)	736 (79%)	973 (70%)	4153 (78%)
Dominant Positive/Negative dipole for filtered samples (%)	65/35	78/22	87/13	79/21	52/48	73/27
#Filtered Flashes	15,882	26,764	62,393	27,991	80,238	213,268
# Filtered <i>Chargepol</i> flashes (% of filtered flashes)	49	44	47	42	35	41

of updrafts. One could criticize the classification of the sample between 1242 and 1252 UTC as only 1 of the 5 flashes recorded during that period is analyzed by *Chargepol* algorithm (Figure 1a) leading to a confidence ratio equal to the 20% threshold. A dominant positive dipole is deduced for the entire sample while there are in fact 3 flashes not analyzed by *Chargepol* algorithm in the lower part of the cloud (probably $-ICs$) for 2 flashes in the upper part of the cloud (potential $+ICs$) with only one of them used for charge layer retrieval. If all the flashes had been analyzed, the sample would have been classified as a dominant negative dipole sample with a dominant positive layer at the bottom. This rare (4% of samples with a confidence ratio smaller or equal to 25% and composed of less than 11 flashes) type of sample is a source of error for the study but the statistical analysis of the samples and the different filters applied on the samples allow to reduce its impact on the charge structure classification.

3. Results and Discussion

3.1. 5-Month Distribution of Electrical Cells Recorded in Corsica

During the 5-month period (June to October 2018) within the SAETTA domain, 711 electrical cells with at least 20 flashes and lasting more than 20 min were identified by ECTA during 79 different days. About 73% of the flashes detected by the LMA over the 5-month period are included in the electrical cell data set. Table 1 provides several statistics per month and for the entire period, while Figure 2 presents the maps of the cell trajectories per month. The most prolific month was August with 229 cells (Table 1; Figure 2c) followed by October with 189 cells (Table 1; Figure 2e). The month with the least number of cells was July with only 77 cells (Table 1; Figure 2b). The cells are typically found over land during the summer months (Figures 2a–2c) with a maximum number of cells in August. For the months of September and October (Autumn) the cells are mostly located over the sea (Figures 2d and 2e). The summer cells of the study seem to be induced by orographic forcing on the Corsican relief, and are rather stationary with short chaotic trajectories. In autumn, the cells are rather located over the sea with longer and more straight tracks. This agrees with Galanaki et al. (2018) who show that summer thunderstorms in the Mediterranean region take place rather over land, in the afternoon and especially over the reliefs triggered by orographic lifting. They also argue that autumn Mediterranean thunderstorms are essentially on the sea around the coasts, regardless of the time of day with a convection favored by the instability created by flows of colder continental air masses on a still relatively warm sea.

The two major weather events with the highest number of cells occurred between August 14th and August 15th with 73 individuals cells and between October 28th and October 29th with a total of 67 cells. The last one was due the ADRIAN storm (Figure 2e, tracks in red) (also called Vaia storm) (Giovannini et al., 2021) that triggered some long-track supercells in a south-western flow that produced intense electrical activity, strong winds and two tornadoes in Corsica. The two major events produced almost a third of the cells in their respective months. Thus it must be taken into account that the statistics for these 2 months are influenced by particular weather events.

The median cell duration of the 711 cells is 59 min with a variation of less than 5 min when considering each month independently. About 25% of the cells lasted more than 1h30, 13% more than 2h and 5% more than 2h40.

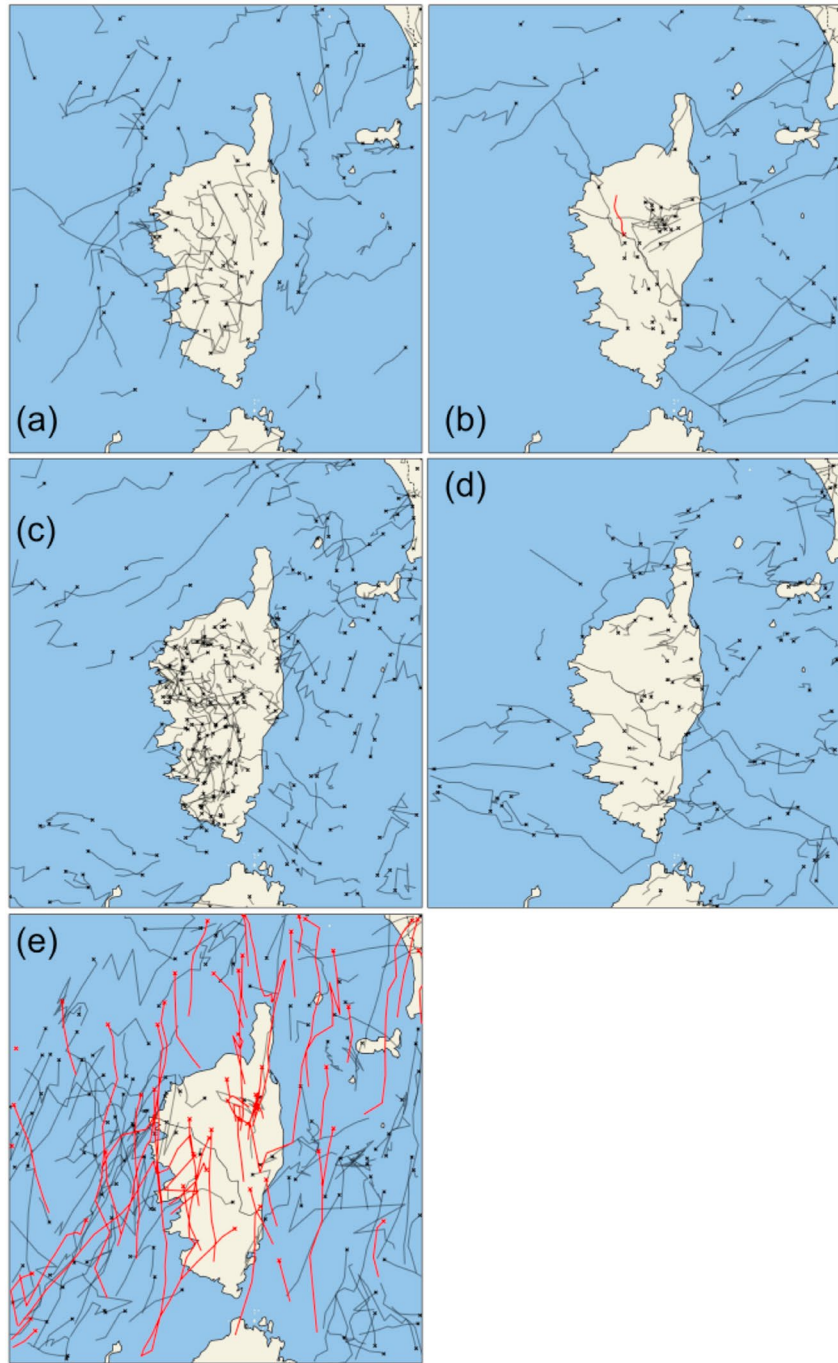


Figure 2. Map of the cell trajectories obtained by ECTA on the SAETTA domain for each month. (a) June 2018. (b) July 2018 with the cell #2 trajectory, taken as an example in Section 2.5 and in the Appendix A, highlighted in red. (c) August 2018. (d) September 2018 and (e) for October 2018 with cells trajectories associated to the ADRIAN situation highlighted in red. Crosses represent the end of the trajectories.

The median number of samples (10-min period) per cell is 6 which is consistent with the median cell duration of 1 hr.

Table 1 details the impact of the filtering of the samples (see Section 2.5) on the sampled database. We recall that the purpose of the filtering is to reduce the uncertainty on the determination of the dominant dipole structure of each sample. Over the 5 months, 22% of the 10-min samples were excluded. The most filtered month is October

with 30% of these samples excluded and the least filtered are July and August with only 17% of their samples excluded. Regarding the dominant dipole structure, the filtering mainly removes the samples without charge structure identified by the *Chargepol* algorithm (Unknown, Table 1). Over the 5 months, 10% of samples were without charge structure, 66% of samples with dominant positive dipole charge structures (DPL above DNL) and 24% of samples with dominant negative dipole charge structures (DPL below DNL). If one only takes into account the samples with an identified charge structure, 73% (27%) of samples were associated to a dominant positive (negative) dipole.

After filtering on samples without charge structure together with samples with low confidence (see Section 2.5), 4,153 samples with a total of 213,268 flashes approximately correspond to 720 hr of lightning activity. Among these flashes, 88,219 (41%) of them were used by the *Chargepol* algorithm to identify a dominant dipole structure per 10-min sample period. The results over the 5 months show a dominance of the occurrence of samples with a dominant positive dipole charge structure (73%) and the filter did not exclude any particular charge structure and kept the observed positive/negative dominant dipole proportions. This dominance has a monthly variation with a percentage between 78% and 87% for the months of July, August and September and lower for June (65%) and October (52%). It suggests that the predominance of summer orographic thunderstorms favors the presence of dominant positive dipole charge structures. On the contrary, in October, thunderstorms are mostly over the sea with conditions more favorable to dominant negative dipole charge structures. Moreover, October is the month with the lower percentage (35%) of analyzed flashes by *Chargepol*. It is assumed that, at this period of the year, the charge layers are less thick and less stratified on the vertical due to the lower vertical development of clouds but also to cells further away from the network preventing of having well defined vertical channels during the early stage of the flashes for an unambiguous classification by *Chargepol*.

It is worth to remember that dominant negative dipole samples are observed throughout the entire study period and that they can occur punctually in the cell lifetime. However dominant negative dipole samples can be the only category of samples observed in certain meteorological conditions like during south-west flow events carrying aerosols (Coquillat et al., 2022). The location of dominant negative dipole samples in Corsica was investigated but no geographic hotspot was found in this 5-month sample database (not shown).

When compared to the percentage of samples found by Medina et al. (2021) in Argentina and the USA, the fraction of dominant negative dipole in Corsica seems more important (Colorado samples being an exception). This may be due to the Corsica environment less conducive to deep convection and dominant positive dipole charge structure but also to the sample duration (10 min here vs. 60 min). Indeed, with a period of 10 min there are more

chance to capture a dominant negative dipole structure more likely during its dynamic dissipation/formation phase or within weak thunderstorms. On the opposite, when a dominant positive dipole charge structure is present, there is generally a strong increase in the flash rate at high altitude. So over a short time interval, the number of flashes in the upper dipole can be much higher than the number of flashes in the lower dipole over a longer period. Thus, at the storm-scale and with samples of 1 hr like Medina et al. (2021), it is very likely that the dominant dipole will be retrieved from the flash population in the upper positive dipole that induces a high flash rate period. With the finer time window of 10 min, there is more chance to better characterize the dynamic within the storm and to detect periods with lower flash rate and with potentially dominant negative dipole charge structures.

3.2. Samples Charge Structure Distribution

In the following, the properties of the lightning activity are discussed relatively to DPL and DNL altitudes (see Section 2.5). Indeed, Figure 3 shows the 2D distribution of DPL-DNL altitude pairs where each 500 m × 500 m bin represents a unique dominant charge structure. As mentioned in Section 2.5, all samples with the same DPL and DNL heights are filtered out. As expected, Figure 3 reveals a wide altitude distribution of charge structures, with DPL (DNL) heights ranging from 1 to 12.5 km (1.5–11 km). In addition, Figure 3 shows that the DPL-DNL charge structures are not uniformly distributed,

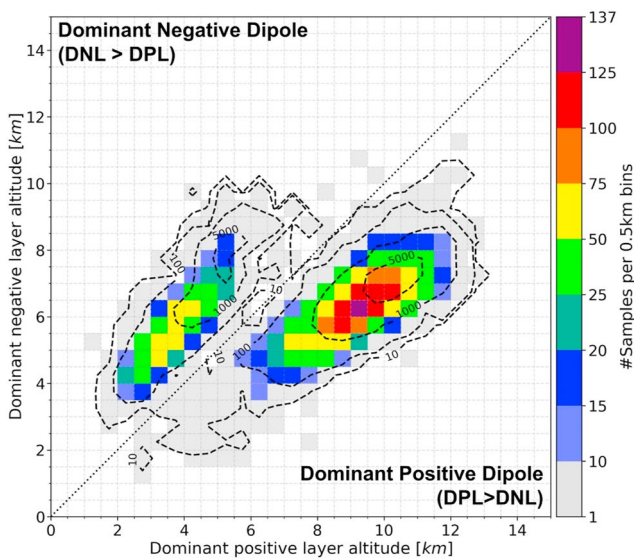


Figure 3. 2D distribution (0.5 km bins) of samples by altitude of their DNL and DPL. Contours show the accumulated number of flashes in bins. The diagonal black dotted line separates dominant positive and negative dipole domains.

some configurations appearing more often than others. There are two main types of charge structure: class #1 with DPLs found globally between 6 and 12 km in altitude with associated DNLs located between 4 and 9 km height, and class #2 composed of DNLs located between 4 and 8 km with associated DPLs between 2 and 6 km altitude. The first (second) configuration corresponds to dominant positive (negative) dipole charge structures with a dominant positive (negative) layer above the dominant negative (positive) layer. In addition, class #1 exhibits a larger vertical range compared to class #2 suggesting that class #2 population is more vertically compact and that class #1 contains dominant charge layers that can be quite distant vertically. In terms of confidence in these dominant dipole distributions, the confidence ratio is generally more than 30% for all DPL-DNL pairs.

For statistical confidence, elements of the 2D distribution with less than 10 samples—469 of the 4153 samples (11%)—are discarded in the analysis, but still plotted in gray in Figure 3. Additionally, 84% of the 213,268 flashes were in bins with at least 10 samples. Among the 3,684 validated samples, 75% (25%) samples belong to class #1 (class #2). By filtering out samples in bins with less than 10 samples, the total number of flashes, the total number of samples and therefore the percentage of dominant positive and negative samples are changed. Indeed, more dominant negative dipole samples than dominant positive ones are filtered out but the order of magnitude between the two classes is rather kept (73%/27% (Table 1) vs. 75%/25%). Bins with less than 10 samples are overall associated with a low cumulative number of flashes as shown by the contours in Figure 3 except for the few dominant negative samples with a DPL located between 6 and 7 km and a DNL found between 7.5 and 9 km where more than 1,000 flashes were summed up. Considering at least 10 samples per bin, the more common dominant dipole charge structure over Corsica and for the 5-month period corresponds to a positive one composed of a DPL between 8.5 and 9 km height with an associated DNL found between 6 and 6.5 km height, representing around 4% of all samples.

Vertical profiles of temperature with balloon soundings are conducted by Météo-France every day at 00 UTC and 12 UTC from Ajaccio (8.73°E–41.91°N). An analysis on 688 samples, located within a 1-degree square centered at the balloon launch facility during the whole study period, and recorded within a 6-hr time window centered at the launch time, revealed that the -40°C isotherm varied between 9 and 10.5 km in altitude, the -10°C isotherm ranged between 5.5 and 6.5 km in altitude while the 0°C isotherm varied between 2 and 4 km in altitude. There were therefore a variation of 1.5–2 km in altitude of isotherms during the study period. The DPL (DNL) distribution peaked around the -40°C (-15°C) isotherm for dominant positive dipoles samples. For dominant negative dipoles samples, DPL (DNL) altitude distribution peaked around the 0°C (-10°C) isotherm. These temperature ranges fit well with those reported by Fuchs et al. (2015) with a dominant positive (negative) charge layer located at around -40°C (-20°C) for normal charge structure but also to those associated to anomalous charge structure with a dominant positive layer situated at the 0°C isotherm.

According to Figure 3, for both dominant positive and negative dipole charge structures the maximum accumulated number of flashes does not necessarily correspond to the bins with the most samples which suggests that the number of flashes and therefore the flash rate per (10-min) sample varies in relation to the charge structure.

3.3. Total Flash Rate According to the Charge Structure

As a reminder, the aim of this study is to characterize the electrical activity associated with different charge structures, here labeled by the dominant dipole. Figure 4 synthesizes the variability of the flash rate per DPL-DNL altitude bins. Each DPL-DNL altitude bin contains at least 10 samples and is composed of a series of 10-min period of lightning activity with different properties. In the following, the flash rate corresponds to the ratio of the number of flashes per minute over the 10-min period and is known for each DPL-DNL altitude pair.

Figure 4b shows the median of the flash rate, for both dominant positive and negative dipole distributions, higher flash rate statistically occurs when the upper layer of the dominant dipole reaches higher altitude. A maximum median flash rate of $42 f \cdot \text{min}^{-1}$ is obtained for dominant negative dipole samples with a DNL located between 8 and 8.5 km height and a DPL found between 5 and 5.5 km, while there is less than 2 to $3 f \cdot \text{min}^{-1}$ for DNL under 5 km and DPL under 8 km. For dominant positive dipole samples, the maximum median flash rate is $20 f \cdot \text{min}^{-1}$ for DPL between 11.5 and 12 km and DNL between 8 and 9 km.

For dominant negative dipole (Figure 4a) samples, the median average flash rate increases with the DNL altitude from $1 f \cdot \text{min}^{-1}$ or less for DNL between 3.5 and 5.5 km height to more than $40 f \cdot \text{min}^{-1}$ for DNL around 8.5 km height. For dominant positive dipole samples (Figure 4c) the flash rate also increases with the DNL altitude

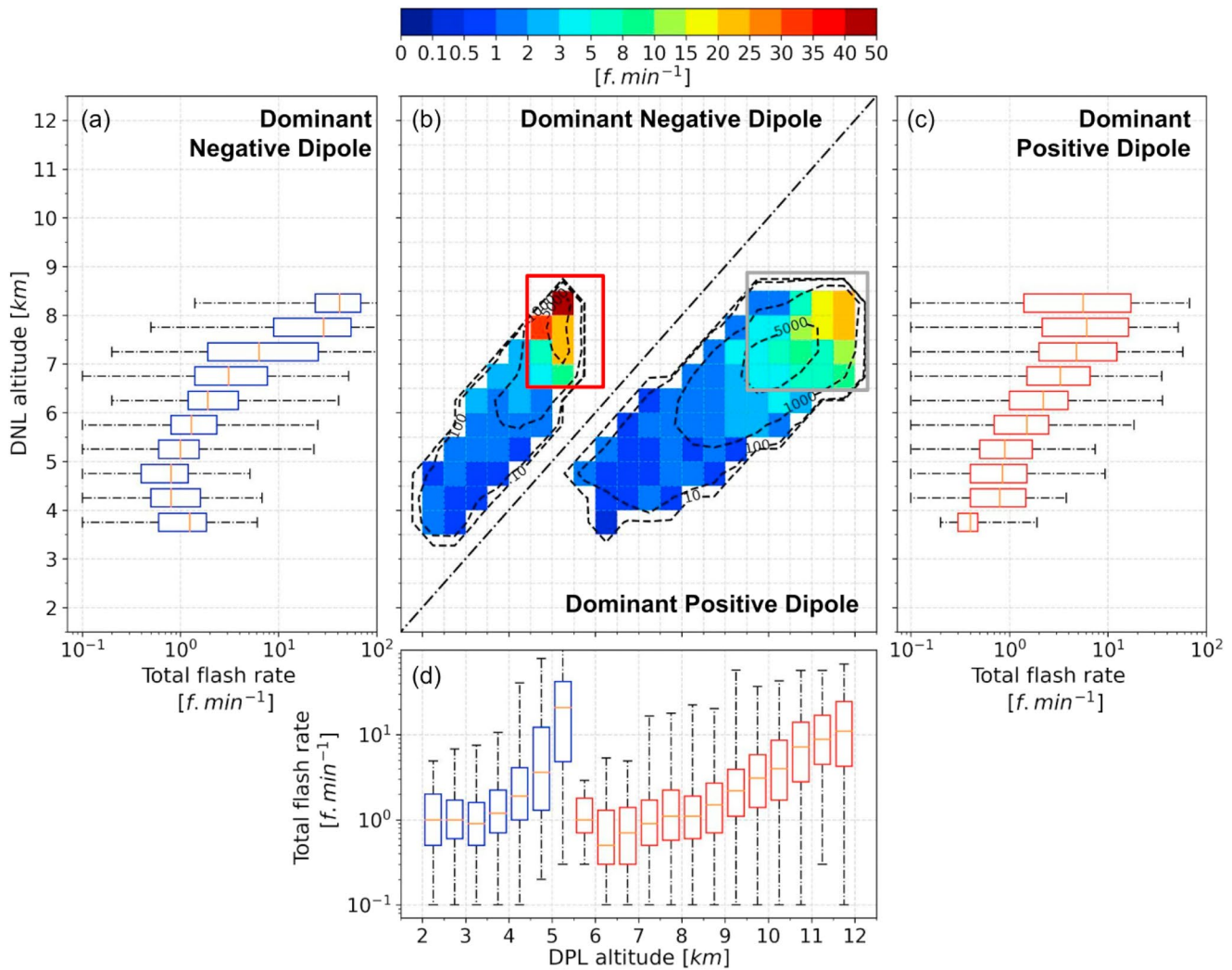


Figure 4. (a) Average flash rate per dominant negative dipole samples in 0.5 km DNL altitude bins. The box extends from the first quartile to the third quartile of the data, with an orange line at the median. (b) 2D distribution (0.5 km bins) of the median of the average flash rate per sample. Contours show the cumulated number of flashes in bins. The diagonal black dotted line separates dominant positive and negative dipole domains. Red and gray boxes separates samples classes. (c) as (a) but for dominant positive dipole samples. (d) Average flash rate per sample in 0.5 km DPL altitude bins.

but less dramatically (up to $20 f. min^{-1}$). For both charge layer populations, the flash rate often ranges over two orders of magnitude (Figures 4a and 4c). The relationship between the DPL altitude and the median average flash rate (Figure 4d) is more complicated with a strong intensification of the flash rate for DPL associated to dominant negative dipole samples (in blue) between 4 and 5.5 km in altitude corresponding to “intense” negative dipole samples. For DPL associated to dominant positive dipole samples (in red, Figure 4d) there is a continuous increase of the flash rate with increasing DPL height between 5.5 and 12 km height.

The increasing trend in the flash rate for dominant negative dipole samples with DPL around 5 km height is comparable to the observations from anomalous Colorado thunderstorms (Fuchs et al., 2015) with a peak flash rate associated with a low dominant positive charge region (temperatures near $-20^{\circ}C$) but also to the observations from anomalous Oklahoma thunderstorms (Fuchs et al., 2015; Lang & Rutledge, 2011). These dominant negative dipole samples with high DPLs altitudes have flash rates comparable to anomalous storms documented by Fuchs et al. (2015) (around $15 f. min^{-1}$) in Colorado but also remain well below the severe anomalous thunderstorms observed by for example, Rutledge et al. (2020) (up to $300 f. min^{-1}$) in the same region. For the present study, the most severe samples (with the strongest flash rate) correspond to dominant negative dipole charge structures with a DNL greater or equal to 6.5 km height and a DPL greater or equal to 4.5 km height (Red box, Figure 4b). These severe samples are relatively rare as they represent 15% of the dominant negative sample population and 4% of

the total sample population. A vast majority of these samples belongs to cells that were recorded during the single special weather event, that is, Adrian storm (Vaia storm; Giovannini et al., 2021) as mentioned in Section 3.1. These samples (Figure 4b, red box) are part of the high altitude negative dipole class. Three others classes are also defined: Low altitude negative dipole class for all the remaining dominant negative dipole samples, high altitude positive dipole class for dominant positive dipole samples with DPL altitudes greater or equal to 10 km and DNL altitudes greater or equal to 6.5 km (gray box, Figure 4b) and low altitude positive dipole class for the all the remaining dominant positive dipole samples.

3.4. Flash Production Relative to the Sample Charge Structure

Since there is a link between flashes rate and charge structures classified thanks to the dominant dipoles, the type of flash produced by each charge structure is investigated here. Figure 5 projects in the DPL-DNL altitude space the IC-CG ratio (a), the positive CG fraction (b) as well as the positive IC fraction (c) according to the different

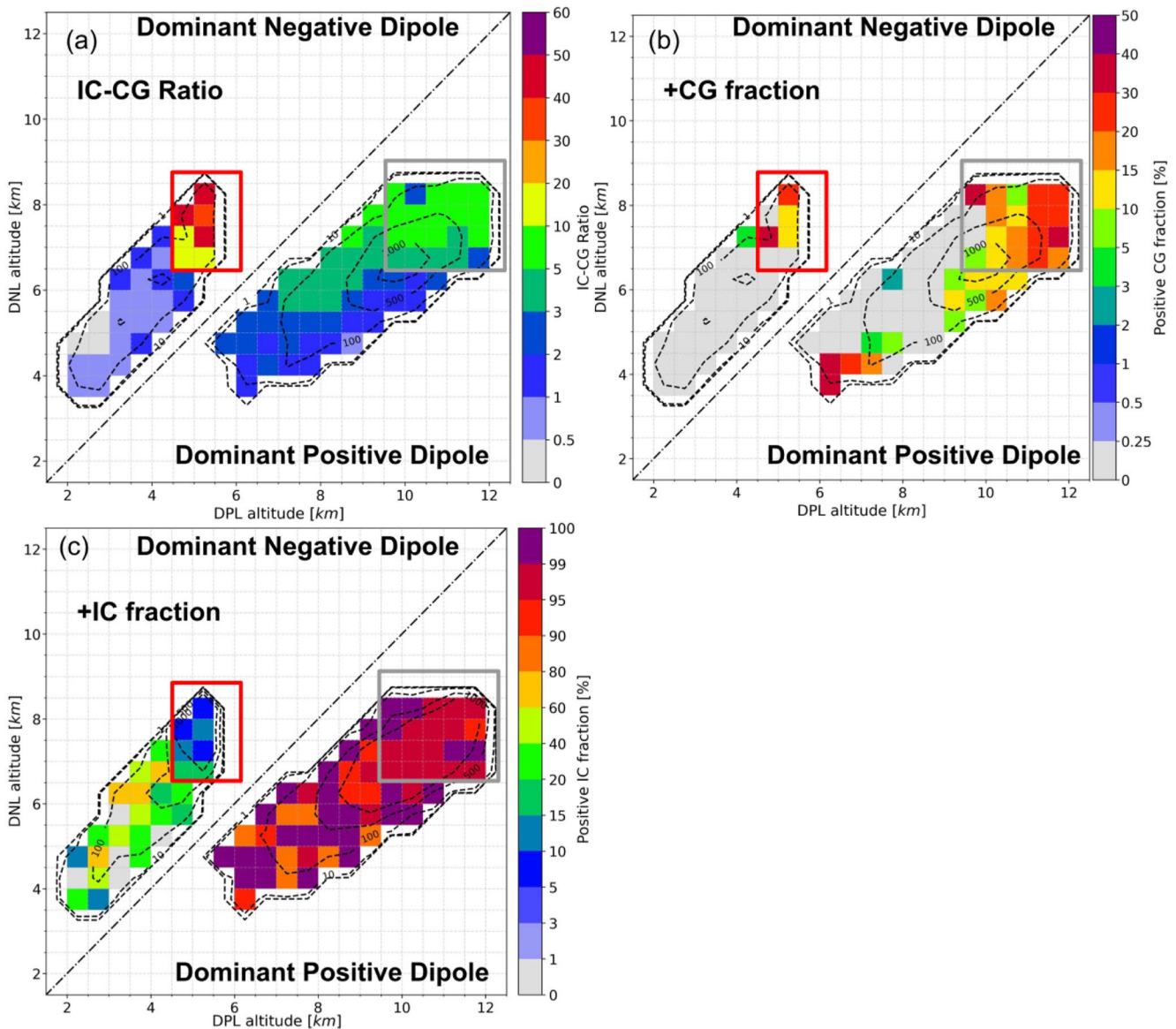


Figure 5. (a) 2D distribution (0.5 km bins) of the median IC-CG ratio of binned samples. Contours show the number of accumulated flashes in bins. The diagonal black dotted line separates dominant positive and negative dipole domains. (b) and (c) same as (a) but for +CG fraction and +IC fraction. Red and gray boxes separate samples classes.

dominant charge structures. For the IC-CG ratio, *LMA only* flashes are also included in the IC population since these flashes are in vast majority small ICs (compact flash) (not shown), not detected by Météorage and typically not qualified by the *Chargepol* algorithm. These ratio and fractions have been calculated per sample, the results discussed here correspond to the median of those parameters for a given DPL-DNL pair. As a reminder, the types and the polarity of *LMA* flashes are obtained by merging *LMA* data to observations from the LF MET network (see Section 2).

$$IC - CG \text{ ratio} = \frac{+IC + -IC + LMA \text{ only}}{+CG + -CG} \quad (1)$$

$$+CG \text{ fraction} = \frac{+CG}{+CG + -CG} \quad (2)$$

$$+IC \text{ fraction} = \frac{+IC}{+IC + -IC} \quad (3)$$

Overall, the IC-CG ratio increases with the altitude of the dominant dipole as does the flash rate (Figure 4b). It is consistent with the results of MacGorman et al. (1989). This ratio is maximum for high altitude negative dipoles samples with 30–50 times more IC flashes than CG flashes. For high altitude positive dipoles, there is rather 5 to 10 times more ICs than CGs. For both dominant positive and negative dipoles, the intense electrical activity is mainly due to intracloud activity for high altitude dipoles with an equivalent contribution between ICs and *LMA only* flashes for dominant positive dipoles samples and an enhanced production of *LMA only* flashes for dominant negative dipoles (not shown). The increased occurrence of these small flashes is consistent with the high flash rates observed, in fact Bruning and Macgorman (2013) have shown an anti-correlation between the size of the flashes and the flash rate. The maximum CG flash rate is observed for these high altitude dipoles (around 3 CG $f. \text{min}^{-1}$) and increases with the height of the dominant positive layer similar to the findings of Salvador et al. (2021) (not shown). Looking at the +CG fraction (Figure 5b), we see that –CGs generally dominate the production of CGs (>90%; <10% for +CGs) regardless of the dominant charge structures except for dominant dipoles associated with high altitude positive dipoles charge structures where from 15% to 40% of the CGs produced are positive. This ratio can nevertheless evolve with the seasons, indeed an increase of the +CG fraction was observed in winter when the clouds have a base at low altitude with a weak vertical extension (not shown).

For the +IC fraction, Figure 5c shows a clear signal of dominance between 80% and 100% of +ICs for all samples with a dominant positive dipole charge structure, result consistent with the flash polarity convention (e.g., Bruning et al., 2014; Medina et al., 2021). On the other hand, for the high altitude negative dipoles samples it is the opposite with a strong dominance of –ICs, also consistent with the flash polarity convention. For low altitude negative dipole samples, there is no clear –IC dominance. This can be explained by the fact that the only few potentially –ICs flashes initiating in this dipole tend to propagate toward the ground and thus to be qualified as –CGs. In summary, referring to the 4 classes defined before, the high altitude negative dipole class is associated with a dominant intracloud activity with mainly –ICs and small flashes (*LMA only*), enhanced –CG and +CG production. Low altitude negative dipole class is associated with mainly –CGs production and some +IC activity. High altitude positive dipole class is associated with a dominance of intracloud activity with strong +ICs and small flashes (*LMA only*) production, enhanced –CG production and the highest +CG production of all the charge structures for the studied data set. Finally, the low altitude positive dipole class produces mainly +ICs and –CGs with the same relative amount.

Overall, charge structures classified as dominant positive or negative dipoles seem to produce at the same time ICs and CGs of both polarities although the intracloud activity remains dominated by flashes of polarity corresponding to that of the dominant dipole. This logically suggests the presence of one or more additional charge layer in the samples, in addition to the dominant dipoles. By investigating the altitude of initiation of the flashes, the presence of others charge layers can be confirmed as detailed in the next section.

3.5. Flashes Initiation Height Relative to the Samples Charge Structure

In the following, the relationship between the flash initiation altitude and the dominant charge structure is studied. A median initiation height is determined for each sample, for each type of lightning (–CG, +CG, +IC, –IC, *LMA only*). For each dominant dipole, we consider that the theoretical flash initiation altitude is located at mid-distance

between the two dominant charge layers (DPL-DNL), in accordance with the model of Kasemir (1960). Figure 6 shows the median of the difference between the median initiation altitude of $-CGs$ and $+ICs$ separately and the theoretical initiation altitude for each DPL-DNL dipole.

For dominant negative dipole samples, the $-CGs$ initiate logically at the theoretical altitude ± 0.5 km (Figure 6a). For dominant positive dipole structures, $-CGs$ typically initiate 0.5–3.5 km below the theoretical initiation altitude of the dominant positive dipole (Figure 6a). This indicates the presence of another layer of positive charges beneath the DNL forming a lower negative dipole (not dominant) in which classical type I $-CGs$ of the Li et al. (2020) classification can initiate. The difference in altitude between the initiation of $-CGs$ in the bottom negative dipole and the theoretical initiation altitude of the flashes in the dominant positive dipole (at the top of the tripole) is supposed to roughly correspond to the thickness of the main negative charge layer. For positive dipoles at low altitudes (DNL around 4 km and DPL around 6 km) with few samples and few $-CGs$ (between 10 and 100 $-CGs$ per bin) it is likely that there is no positive lower layer helping the negative leaders to propagate to the ground as for types I flashes. In such configuration, the $-CGs$ would be rather of type II or III of the Li et al. (2020) classification with a negative leader propagating into the positive layer above (as a $+IC$) and then continues toward the ground. In fact, all types of $-CGs$ are observed at all altitudes for all charge structure but type I flashes are much more common and force statistically the median altitude of $-CGs$ initiation to be in a negative dipole (not shown).

For dominant positive dipole samples, $+ICs$ flashes initiate logically at the theoretical altitude of the bins associated (Figure 6b). For low altitude negative dipole samples, $+ICs$ flashes tend to initiate 0.5–3.5 km above the theoretical initiation height. This indicates the presence of a weak upper positive layer above the dominant negative dipole with $+ICs$ initiating between the main midlevel negative charge layer and the weak upper positive layer. For high altitude negative dipole samples (Figure 6b, red box) the few $+ICs$ flashes initiate at the theoretical altitude or 0.5 km above. Meaning that for these samples, the weak upper positive layer tend to not be present.

LMA only flashes always initiated at the theoretical altitude of the dominant dipoles and $+CGs$ flashes initiated at the same altitude as $+ICs$ (not shown). $-ICs$ generally initiated at the same altitude as $-CGs$ except for samples in the high altitude positive dipole class where the few detected $-ICs$ initiated mostly at the theoretical altitude or up to 0.5 km above. This could be a sign of a presence of a negative upper screening charge layer (e.g., Krehbiel et al., 2008; López et al., 2019; MacGorman et al., 2008) with some $-ICs$ flashes forming between the screening layer and the main dominant positive layer below. This remains a hypothesis due to the low number of $-ICs$

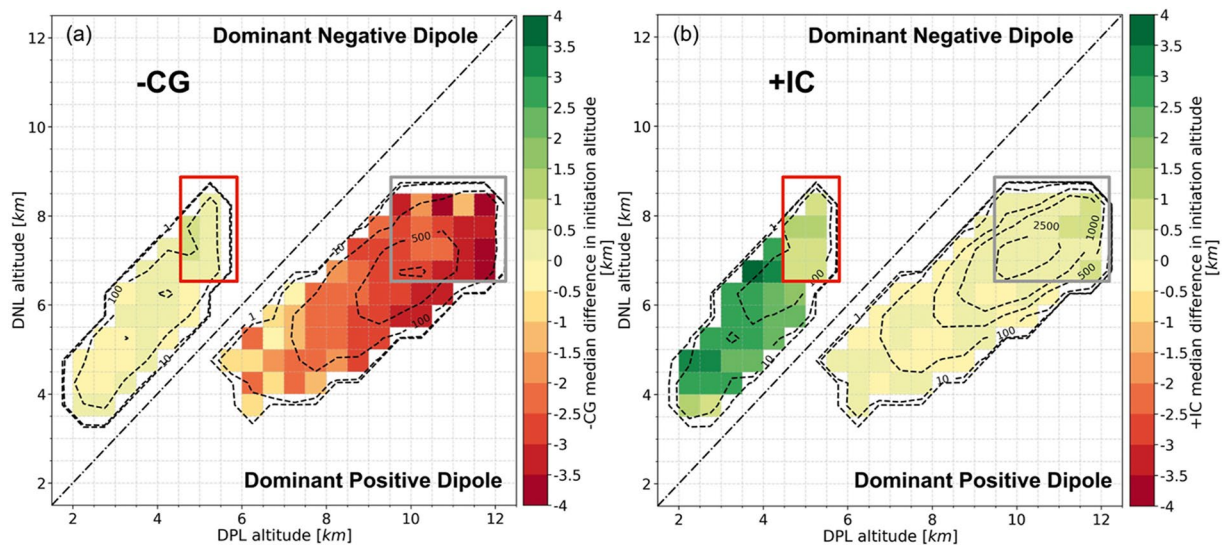


Figure 6. (a) 2D distribution (0.5 km bins) of the median difference between the samples median initiation height of $-CGs$ flashes and the theoretical one of each bin. Contours show the number of accumulated flashes in bins. The diagonal black dotted line separates dominant positive and negative dipole domains. (b) same as (a) but for $+IC$ flashes. Red and gray boxes separate sample classes.

flashes found and because the screenings layer was never clearly visible and detected by *Chargepol* algorithm on the few cells studied by visual inspection.

4. Summary and Conclusion

LMA SAETTA and Météorage lightning records were merged together to characterize the electrical activity of Corsican thunderstorms. LMA flashes were classified according to the concurrent observations from the LFLS Météorage. A cell tracking algorithm on LMA data was used to build a database of electrical cells over a 5-month period from June to October 2018. Different parameters such as flash rate are associated with each electrical cell, this database is then used statistically to deduce properties of Corsican thunderstorms over this period. The application of a new charge layer retrieval algorithm permitted to classify as dominant dipoles the main vertical charge structures per 10-min period for each individual electrical cell. The charge layer retrieval and the cell separation in 10-min periods was discussed for one electrical cell recorded on the 28 July 2018. The studied cell exhibited a dominance of positive dipole charge structure according to *Chargepol* algorithm that could be translated into a normal tripole charge structure by taking into account the non-dominant lower negative dipole.

A statistical study has been performed on a data set composed of 711 electrical cells divided in samples of 10 min for identification of the altitudes of dominant negative and positive layers. We recall that the population of electrical structures considered in this study does not take into account electrical cells with a lifetime of less than 20 min and with a total lightning activity of less than 20 flashes. After filtering out samples with low confidence, a total of 3,684 samples were classified according to their dominant dipole. For this 5-month period study, about 25% (75%) of the samples had a dominant negative (positive) dipole charge structure. Samples associated to dominant positive dipole can be classified as normal samples since the dominant charge structures recall the normal dipole charge structures (Dye, 1986; E. R. Williams, 1985). These normal samples also recall the normal tripole charge structure (E. R. Williams, 1989) since the upper positive charge layer of the normal tripole structure is more electrically active than the lower positive layer (Lang & Rutledge, 2011) meaning that the upper positive dipole is the dominant one. This does not prevent the presence in these samples of some flashes propagating in a potential negative dipole indicating the presence of a low-level non-dominant positive layer. On the opposite, samples with dominant negative dipole can be classified as anomalous samples since the dominant charge structure looks like a negative dipole charge structure (e.g., Bruning et al., 2007; Qie et al., 2005; Salvador et al., 2021). Here too, this does not prevent the presence of some flashes in a potential positive dipole indicating the presence of an upper non-dominant positive layer. It also reminds the bottom-heavy charge structure (e.g., Bruning et al., 2007; Mansell et al., 2010) which is a normal tripole with a dominant activity in the lower part of the storm (negative dipole) and few flashes occurring in the positive dipole. Although this study shows a wide variability in the height of the dominant positive and negative layers observed, the most frequent dominant positive layer altitude associated with a normal (anomalous) charge structure is located around 10 km (3 km) high, altitudes consistent with the observations of Salvador et al. (2021) for example, On a smaller population of samples with radio-sounding temperatures profiles close in time and space, the present study gives dominant positive layers located at temperatures around -40°C (0°C) for normal (anomalous) charge structures in agreement with the results of Fuchs et al. (2015).

These statistical results only represent a 5-month period composed of 79 different days with lightning activity. It should be stressed out that the results obtained for August and October 2018 are mainly driven by two major weather situations that produced almost one third of the total electrical cell number of each month. The relatively high proportion of dominant negative (positive) dipole for October 2018 (August 2018) could then be explained by the high number of cells and the weather conditions associated with these extreme events. The study also relies on the notion of samples, which ultimately provides a snapshot of the charge layer structures during a given period set to 10 min in the present study. These charge structures, as retrieved in this work, are mainly representative of bi-level lightning flashes, with a well-defined initial vertical propagation phase meeting the analysis criteria of the *Chargepol* Algorithm. The classification of the samples by counting flashes in each dipole can therefore vary with the temporal position of the 10-min time window relatively to the lifecycle of a given electrical cell, and especially in the case of cells with low flash rates. It is believed that a statistical study on a large number of samples in addition to the different filters applied on both the samples and the LMA data as described in this study can reduce the impact of this arbitrary time window on the classification of dominant dipole charge structures.

Several macroscopic electrical parameters such as flash rate, IC-CG ratio, +CG fraction, +IC fraction and flash initiation height have been analyzed according to the charge structure. This study confirms that the higher in altitude the dominant dipole is, the higher the flash rate is for both anomalous (dominant negative dipole) and normal (dominant positive dipole) charge structures. In this study, a certain population (high altitude negative dipole) of anomalous charge structures produced the highest flash rate and were linked to severe weather (strong winds, supercells). However, with regard to these samples, it would seem that Corsican thunderstorms, associated to dominant negative dipoles, do not predominantly produce positive CGs and the use of this criterion can therefore not be applied for the identification of anomalous charges structures in Corsica.

The charge structures have been classified in 4 classes according to the polarity and the height of the dominant dipole. These 4 classes are summarized in a conceptual scheme (Figure 7). In general, the most frequent class of charge structures (in terms of 10 min periods) is the low altitude positive dipole class that represent about 58% of the samples. Storm periods with such charge structures exhibit a low flash rate ($0.5\text{--}3 \text{ flash. min}^{-1}$) with mainly +IC flashes occurring in the dominant upper positive dipole and -CG flashes in the lower negative dipole. The less frequent category (4%) in Corsica, the high altitude negative dipole class, produces the highest flash rate ($20\text{--}50 \text{ flash. min}^{-1}$). The dominant negative dipole of this class is located above 4 km height and produced essentially -IC flashes, short duration flashes and few -CGs. The third category, named high altitude positive dipole class, is associated with a large production of +IC flashes and an enhanced production of CG flashes of both polarities since these charge structures are responsible of the highest CG flash rate observed ($3 \text{ CG flash. min}^{-1}$). Finally, the fourth and last category, called low altitude positive class, represents about 21% of the samples and produces mainly -CGs and -ICs with some +IC activity.

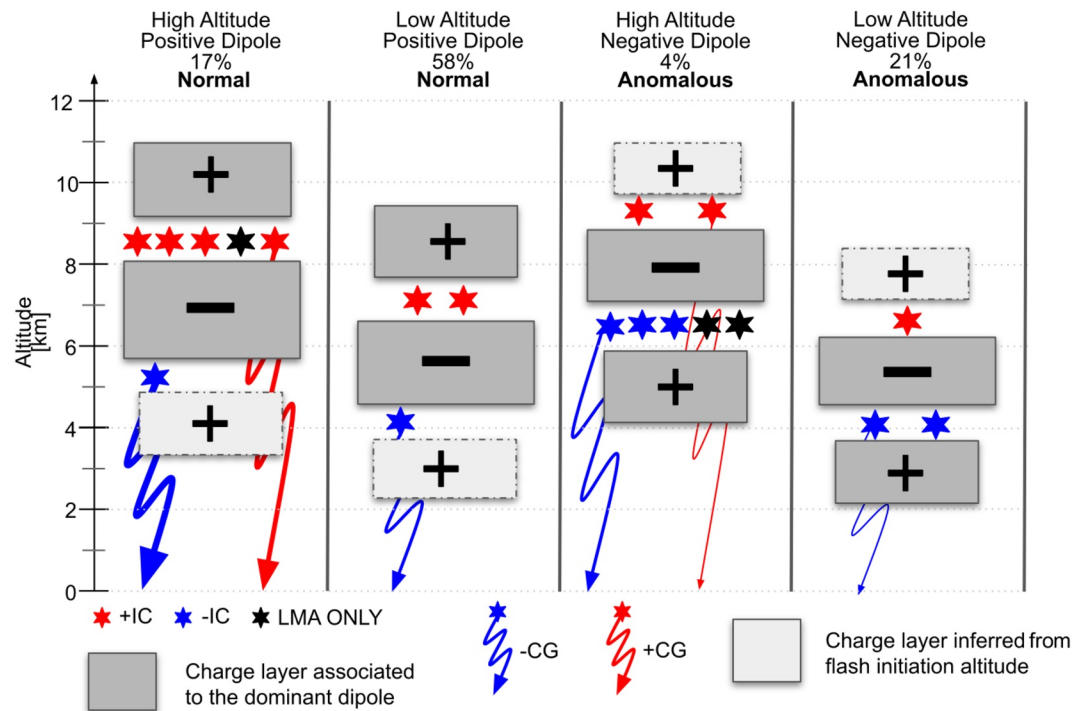


Figure 7. Conceptual scheme of the four different charge structures classes (dominant dipole in samples) observed in Corsica over the 5 months and the main flash production associated. Samples frequency of each class are given (%). Number of icons denote the relative number of flashes occurring between layers. CG icons with a thicker line symbolize an enhanced CG activity. Charge layers with dashed lines are not always present.

The wide ranges of charge structures observed should depend on the meteorological conditions influencing the charge distribution but also on the period in the life cycle of a storm. In the context of this study, the goal was to document the lightning flashes produced by the different observed charge structures and not to link these charge structures to typical environmental conditions. Aerosol content (Coquillat et al., 2022) and cloud base height (Fuchs et al., 2015) are examples of assumptions about environmental conditions that could promote dominant negative dipole and anomalous charge structures throughout the life of the storm. The other hypothesis is that thunderstorm life cycles influence the observed charge structures. The analysis of the occurrence of charge structures in the life cycle of their respective cells did not give any (strong) signal validating this hypothesis, only high altitude positive dipole class tend to occur mostly at the mid-life of the cells (not shown).

The synergistic use of VHF LMA and LF LLS observations gives a rational type and polarity classification to LMA flashes with regard to the vertical charge structures and the flash initiation heights. The automatic identification of vertical charge structure gives important information about storms dynamics and electrical activity that can be use for storm monitoring. Information on the meteorological parameters associated with each charge structure could be useful in order to identify the conditions conducive to anomalous thunderstorms in the North-Western Mediterranean Sea in comparison to anomalous thunderstorms in the US Great Plains for example. The influence of the land/sea transition of thunderstorm cells on their charge structure should also be investigated.

Appendix A: Electrical Cell Tracking Algorithm (ECTA)

The algorithm works through the following 4 successive steps:

- 1) A 2D density of individual L2b flashes (FED; Flash Extent Density) during 5 min in a pixel of 1 km² is computed first (see pixels on an example Figure A1a and A1b). This calculation is updated every minute. We use a FED instead of a VHF sources density since the number of sources reconstructed by the LMA network decreases with the distance of the cell from the network center (Thomas et al., 2004), the “LMA flash” object is being less sensitive to this distance.

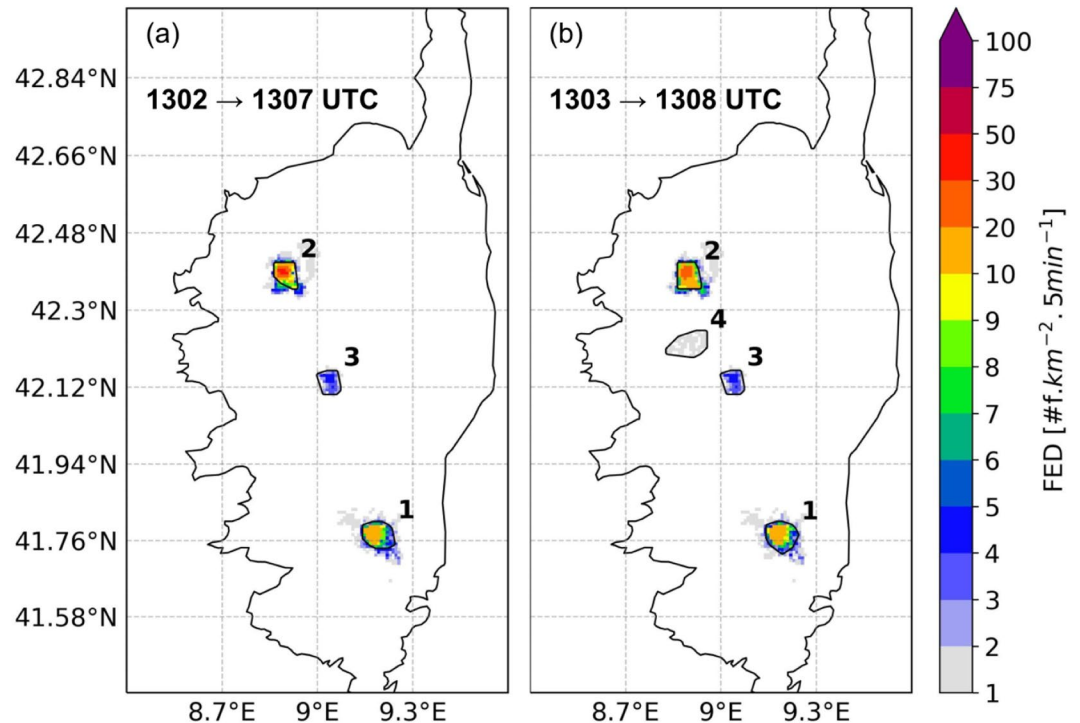


Figure A1. Flash extent density (FED) and clusters borders with identification number obtained with ECTA on the 26 July 2018 from (a) 1302 to 1307 UTC and (b) 1303 to 1308 UTC.

- 2) FED clusters are then identified within a given 5-min period by an application of two successive DBSCAN (Pedregosa et al., 2011) methods on pixels: The first DBSCAN pass aims at separating clusters according to a certain euclidean distance and to a specific threshold on FED. Here, all pixels are taken into account with a minimum FED value of 1. Two clusters belong to the same electrical cell if the distance between the closest pixels of the two given clusters is less than 10 km. This distance was selected based on a sensibility study (not shown) and is similar to the one used by Fuchs et al. (2015) for the identification of adjacent cells as isolated cells, and to the distance threshold used by Galanaki et al. (2018) for cell clustering using the ZEUS lightning sferics network.

Depending on the structure of the parent cloud, the clusters may spread horizontally because of the propagation of lightning flashes in the stratiform part of the storms (Carey et al., 2005; Coquillat et al., 2019; Weiss et al., 2012). Electrical cells can have distant convective centers but close (<10 km) or even connected stratiform regions. In this case, the first DBSCAN pass will gather two cells under the same cluster. To solve this problem a second DBSCAN algorithm is applied on the existing clusters with a threshold on FED to identify and select the most electrically active regions. It uses an adaptive threshold proportional to the maximum FED of each cluster identified by the first DBSCAN pass. We consider that the maximum flash density pinpoints the convective core of the cell (e.g., Bruning & Macgorman, 2013; Calhoun et al., 2013) while the stratiform region of the cluster corresponds to pixels having a FED lower than 25% of the max FED of the cluster (value chosen after tests, not shown). This adaptive threshold, constant in percentage (25%) but variable in actual FED value, is cluster dependent and prevent using a single fixed threshold since, at the same time, different clusters can exhibit maximum FED values which may differ significantly.

The second DBSCAN pass works like the first one and with the same euclidian distance of 10 km but it is applied on each cluster individually with the pixels selected after adaptive threshold. In most cases, it just restricts the clusters borders to the convective part and reduces the horizontal size of the clusters. But in the case of a large cluster with two (or more) convective cores connected through low FED pixels, the second DBSCAN pass will separate the cluster into 2 (or more) new clusters with contours closer to the convective (electrical) core. Figure A1a shows an example of the separation of the FEDs into clusters at an instant T with their borders delimiting their respective most active region due to the second DBSCAN pass.

- 3) At the end of the second step, for each minute, all clusters possess an identification (ID) number and their borders are defined with a polygon. As the process of identification of the cells is completed, the tracking of the cells over time has to be performed. The polygons formed by the clusters are compared two by two to detect cluster overlapping. Indeed, if there is any geographical overlap between a polygon at time T+1 (son) with a polygon at time T (father) then the son cluster is considered as the future of the father cluster and takes father's ID. In addition integrating over 5 min the lightning data and using simultaneously a sliding time window, avoid creating non-overlapping cells especially for fast-moving storms. In its present configuration, with the 5 min integrated density, 4 min of electrical activity are always in common for two successive FED images. As an example, Figure A1a and A1b show clusters identified at two successive time steps, clusters #1,#2 and #3 at 1307 UTC (Figure A1a) and clusters #1, #2, #3 and #4 at 1308 UTC (Figure A1b). The clusters keep the same identification number (clusters #1, #2 and #3) because there are geographical overlaps between the two time steps. Cluster #4 is considered as a new one as it does not overlap any other cluster.

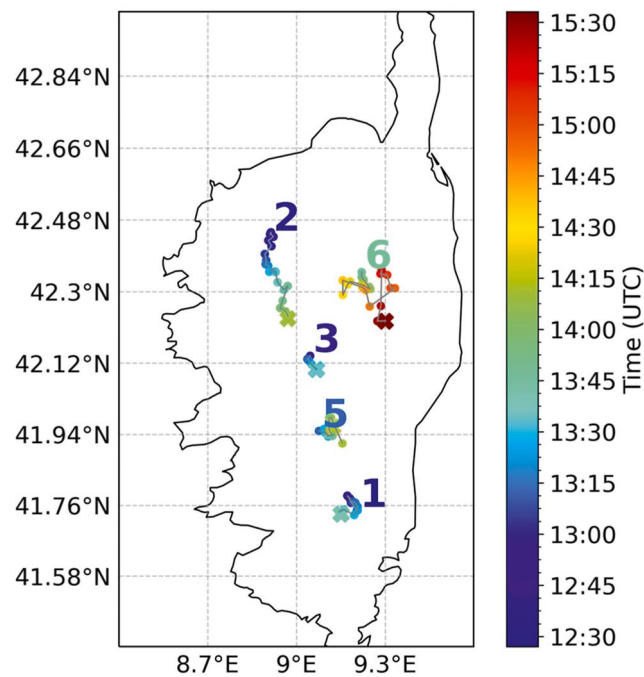


Figure A2. Cells identification numbers and trajectories identified by the ECTA algorithm on the 26 July 2018. Trajectories are colored with time (circles) and crosses indicate the end of the trajectories. Only cells with a minimum of 20 flashes and a minimum duration of 20 min are shown.

Complicated cases can appear, in particular the cases where cells split or merge. If a mother cell has several daughter cells (split), the daughter with the largest overlap area with the mother cell takes the ID number of the mother. The other daughter cells are considered as new cells. In case several mother cells merge into one daughter cell, the mother cell with the largest area of overlap with the daughter cell provides its ID number, and the other mother cells are no longer considered active. The contour of any cell that is no longer active is still kept in memory for 20 min after its last electrical activity in order to revive it if a new electrical activity reappears and overlaps the old position of that cell. At the end of step 3, the electrical activity of a day over the domain of interest is composed of cells, each cell labeled by an ID number and geo-located by its position (centroid) and its border at each time step of its life. For example, Figure A2 shows the cells along with the trajectories obtained by ECTA for the day of 26 July 2018.

- 4) The last step extracts all the L2b flash data that belong to a given electrical cell. Any flash with its initiation located within the contour of a given cell is extracted. We consider that the flashes are initiated preferentially in the convective part of the storm. Indeed Ribaud et al. (2016) showed that 97% of the first VHF sources of the flashes were initiated in the convective regions. The extraction by flash-object instead of by sources allows to recover data outside the surface defined by the contour of the convective cell. Figure A3 shows an example of an extraction of L2b data associated to one single cell (cell #2, 26 July 2018).

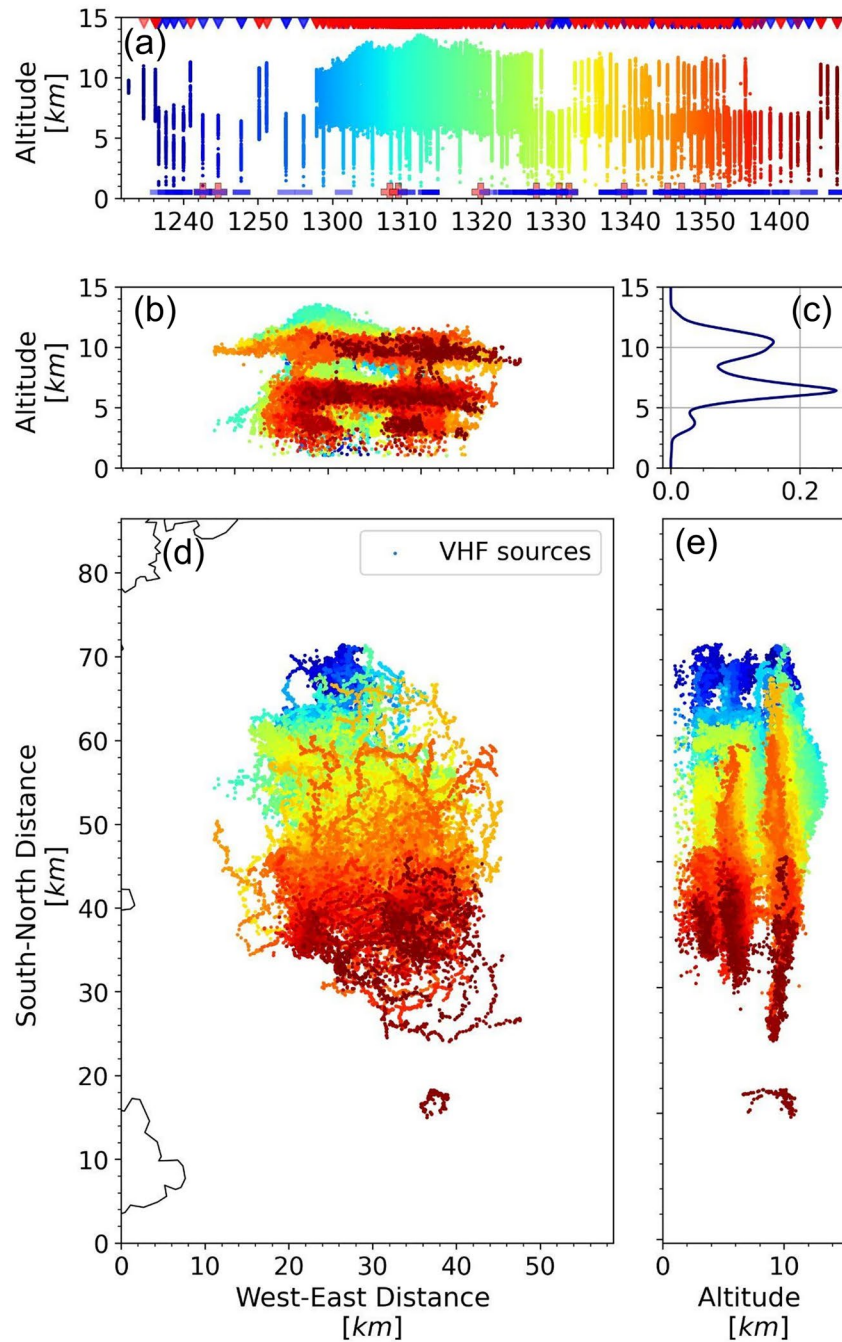


Figure A3. LMA and MET data extracted from ECTA for the cell #2 of 26 July 2018. VHF sources are colored with time. (a) VHF sources altitude versus time (UTC). (b) VHF sources altitude versus longitude. (c) VHF sources altitude histogram. (d) VHF sources altitude 2D projection. (e) VHF sources altitude versus latitude. MET observations for the cell are also added on (a) with IC pulses plotted at 14.5 km height and strokes at 0.5 km height (red for positive currents and blue for negative currents).

Data Availability Statement

The EXAEDRE L2b SAETTA-Meteorage data (Defér et al., 2023) are available on <https://doi.org/10.25326/542#v02>. Météo-France radiosoundings are publicly accessible and are available on https://donneespubliques.meteofrance.fr/?fond=produit&id_produit=97&id_rubrique=33. The scripts used to process the L2b data are available at https://github.com/houelr/ESS_L2b_Scripts.

Acknowledgments

This work is part of the PhD thesis of Ronan Houël funded by SDU2E Doctorate School at University Paul Sabatier (Toulouse). The ANR-16-CE04-0005 EXAEDRE project, the CNES SOLID project and the HyMeX program supported this work. The EXAEDRE-L2b SAETTA-Meteorage Science database is maintained by the French national center for Atmospheric data and services AERIS.

References

Betz, H.-D., Schmidt, K., Fuchs, B., Oettinger, W. P., & Höller, H. (2007). Cloud lightning: Detection and utilization for total lightning measured in the VLF/LF regime. *Journal of Lightning Research*, 2, 1–17.

Betz, H. D., Schmidt, K., Laroche, P., Blanchet, P., Oettinger, W. P., Defer, E., et al. (2009). LINET—An international lightning detection network in Europe. *Atmospheric Research*, 91(2–4), 564–573. <https://doi.org/10.1016/J.ATMOSRES.2008.06.012>

Biagi, C. J., Cummins, K. L., Kehoe, K. E., Philip Krider, E., Biagi, C., Cummins, K. L., & Krider, E. P. (2007). National lightning detection network (NLDN) performance in southern Arizona, Texas, and Oklahoma in 2003–2004. *Journal of Geophysical Research*, 112(D5), 5208. <https://doi.org/10.1029/2006JD007341>

Bruning, E. C., & Macgorman, D. R. (2013). Theory and observations of controls on lightning flash size spectra. *Journal of the Atmospheric Sciences*, 70(12), 4012–4029. <https://doi.org/10.1175/JAS-D-12-0289.1>

Bruning, E. C., Rust, W. D., Macgorman, D. R., Biggerstaff, M. I., & Schuur, T. J. (2010). Formation of charge structures in a supercell. *Monthly Weather Review*, 138(10), 3740–3761. <https://doi.org/10.1175/2010MWR3160.1>

Bruning, E. C., Rust, W. D., Schuur, T. J., MacGorman, D. R., Krehbiel, P. R., & Rison, W. (2007). Electrical and polarimetric radar observations of a multicell storm in TELEX. *Monthly Weather Review*, 135(7), 2525–2544. <https://doi.org/10.1175/MWR3421.1>

Bruning, E. C., Weiss, S. A., & Calhoun, K. M. (2014). Continuous variability in thunderstorm primary electrification and an evaluation of inverted-polarity terminology. *Atmospheric Research*, 135–136, 274–284. <https://doi.org/10.1016/j.atmosres.2012.10.009>

Calhoun, K. M., Macgorman, D. R., Ziegler, C. L., & Biggerstaff, M. I. (2013). Evolution of lightning activity and storm charge relative to dual-Doppler analysis of a high-precipitation supercell storm. *Monthly Weather Review*, 141(7), 2199–2223. <https://doi.org/10.1175/MWR-D-12-00258.1>

Carey, L. D., & Buffalo, K. M. (2007). Environmental control of cloud-to-ground lightning polarity in severe storms. *Monthly Weather Review*, 135(4), 1327–1353. <https://doi.org/10.1175/MWR3361.1>

Carey, L. D., Murphy, M. J., McCormick, T. L., & Demetriades, N. W. (2005). Lightning location relative to storm structure in a leading-line, trailing-stratiform mesoscale convective system. *Journal of Geophysical Research*, 110(D3), 1–23. <https://doi.org/10.1029/2003JD004371>

Chmielewski, V. C., & Bruning, E. C. (2016). Lightning Mapping Array flash detection performance with variable receiver thresholds. *Journal of Geophysical Research: Atmospheres*, 121(14), 8600–8614. <https://doi.org/10.1002/2016JD025159>

Chmielewski, V. C., Bruning, E. C., & Ancell, B. C. (2018). Variations of thunderstorm charge structures in west Texas on 4 June 2012. *Journal of Geophysical Research: Atmospheres*, 123(17), 9502–9523. <https://doi.org/10.1029/2018JD029006>

Coquillat, S., Defer, E., De Guibert, P., Lambert, D., Pinty, J. P., Pont, V., et al. (2019). SAETTA: High-resolution 3-D mapping of the total lightning activity in the Mediterranean Basin over Corsica, with a focus on a mesoscale convective system event. *Atmospheric Measurement Techniques*, 12(11), 5765–5790. <https://doi.org/10.5194/amt-12-5765-2019>

Coquillat, S., Pont, V., Lambert, D., Houel, R., Pardé, M., Kreitz, M., et al. (2022). Six years of electrified convection over the island of Corsica monitored by SAETTA: General trends and anomalously electrified thunderstorms during African dust south flow events. *Atmospheric Research*, 275, 106227. <https://doi.org/10.1016/J.ATMOSRES.2022.106227>

Cummins, K. L., & Murphy, M. J. (2009). An overview of lightning locating systems: History, techniques, and data uses, with an in-depth look at the U.S. NLDN. *IEEE Transactions on Electromagnetic Compatibility*, 51(3–1), 499–518. <https://doi.org/10.1109/TEMC.2009.2023450>

Cummins, K. L., Murphy, M. J., Bardo, E. A., Hiscox, W. L., Pyle, R. B., & Pifer, A. E. (1998). A combined TOA/MDF technology upgrade of the U.S. National lightning detection network. *Journal of Geophysical Research*, 103(D8), 9035–9044. <https://doi.org/10.1029/98JD00153>

Defer, E., Prieur, S., & Pedeboy, S. (2023). EXAEDRE-L2b SAETTA-meteorage science data [Dataset]. <https://doi.org/10.25326/542#v02>

Deierling, W., Petersen, W. A., Latham, J., Ellis, S., & Christian, H. J. (2008). The relationship between lightning activity and ice fluxes in thunderstorms. *Journal of Geophysical Research*, 113(D15), 15210. <https://doi.org/10.1029/2007JD009700>

Dixon, M., & Wiener, G. (1993). TITAN: Thunderstorm identification, tracking, analysis, and nowcasting—A radar-based methodology. *Journal of Atmospheric and Oceanic Technology*, 10(No. 6), 785–797. [https://doi.org/10.1175/1520-0426\(1993\)010<0785:TTITAA>2.0.CO;2](https://doi.org/10.1175/1520-0426(1993)010<0785:TTITAA>2.0.CO;2)

Dotzek, N., Rabin, R. M., Carey, L. D., MacGorman, D. R., McCormick, T. L., Demetriades, N. W., et al. (2004). Lightning activity related to satellite and radar observations of a mesoscale convective system over Texas on 7–8 April 2002. *Atmospheric Research*, 76(1–4), 127–166. <https://doi.org/10.1016/J.ATMOSRES.2004.11.020>

Dye, J. E., Jones, J. J., Winn, W. P., Cerni, T. A., Gardiner, B., Lamb, D., et al. (1986). Early electrification and precipitation development in a small, isolated Montana cumulonimbus. *Journal of Geophysical Research*, 91(D1), 1231–1247. <https://doi.org/10.1029/JD091iD01p01231>

Fuchs, B. R., Bruning, E. C., Rutledge, S. A., Carey, L. D., Krehbiel, P. R., & Rison, W. (2016). Climatological analyses of LMA data with an open-source lightning flash-clustering algorithm. *Journal of Geophysical Research: Atmospheres*, 121(14), 8625–8648. <https://doi.org/10.1002/2015JD024663>

Fuchs, B. R., Rutledge, S. A., Bruning, E. C., Pierce, J. R., Kodros, J. K., Lang, T. J., et al. (2015). Environmental controls on storm intensity and charge structure in multiple regions of the continental United States. *Journal of Geophysical Research: Atmospheres*, 120(13), 6575–6596. <https://doi.org/10.1002/2015JD023271>

Fuchs, B. R., Rutledge, S. A., Dolan, B., Carey, L. D., & Schultz, C. (2018). Microphysical and kinematic processes associated with anomalous charge structures in isolated convection. *Journal of Geophysical Research: Atmospheres*, 123(12), 6505–6528. <https://doi.org/10.1029/2017JD027540>

Galanaki, E., Lagouvardos, K., Kotroni, V., Flaounas, E., & Argiriou, A. (2018). Thunderstorm climatology in the Mediterranean using cloud-to-ground lightning observations. *Atmospheric Research*, 207, 136–144. <https://doi.org/10.1016/j.atmosres.2018.03.004>

Gatlin, P. N., & Goodman, S. J. (2010). A total lightning trending algorithm to identify severe thunderstorms. *Journal of Atmospheric and Oceanic Technology*, 27(1), 3–22. <https://doi.org/10.1175/2009JTECHA1286.1>

Giovannini, L., Davolio, S., Zaramella, M., Zardi, D., & Borga, M. (2021). Multi-model convection-resolving simulations of the October 2018 Vaia storm over Northeastern Italy. *Atmospheric Research*, 253, 105455. <https://doi.org/10.1016/J.ATMOSRES.2021.105455>

Goodman, S. J., Buechler, D. E., Wright, P. D., & David, W. (1988). NOAA/ERL/National severe storms laboratory, Norman, Oklahoma. *Geophysical Research Letters*, 15(11), 1185–1188. <https://doi.org/10.1029/gl015i011p01185>

Houston, A. L., Lock, N. A., Lahowetz, J., Barjenbruch, B. L., Limpert, G., & Oppermann, C. (2015). Thunderstorm Observation by Radar (ThOR): An algorithm to develop a climatology of thunderstorms. *Journal of Atmospheric and Oceanic Technology*, 32(5), 961–981. <https://doi.org/10.1175/JTECH-D-14-00118.1>

Jayarathne, E. R., Saunders, C. P. R., & Hallett, J. (1983). Laboratory studies of the charging of soft-hail during ice crystal interactions. *Quarterly Journal of the Royal Meteorological Society*, 109(461), 609–630. <https://doi.org/10.1256/smsqj.46110>

Kasemir, H. W. (1960). A contribution to the electrostatic theory of a lightning discharge. *Journal of Geophysical Research*, 65(7), 1873–1878. <https://doi.org/10.1029/JZ065i007P01873>

- Krehbiel, P. R., Rioussset, J. A., Pasko, V. P., Thomas, R. J., Rison, W., Stanley, M. A., & Edens, H. E. (2008). Upward electrical discharges from thunderstorms. *Nature Geoscience*, *1*(4), 233–237. <https://doi.org/10.1038/ngeo162>
- Lambert, D., Mallet, M., Ducrocq, V., Dulac, F., Gheusi, F., & Kalthoff, N. (2011). CORSiCA: A mediterranean atmospheric and oceanographic observatory in Corsica within the framework of HyMeX and ChArMeX. *Advances in Geosciences*, *26*, 125–131. <https://doi.org/10.5194/ADGEO-26-125-2011>
- Lang, T. J., Ávila, E. E., Blakeslee, R. J., Burchfield, J., Wingo, M., Bitzer, P. M., et al. (2020). The relampago lightning mapping array: Overview and initial comparison with the geostationary lightning mapper. *Journal of Atmospheric and Oceanic Technology*, *37*(8), 1457–1475. <https://doi.org/10.1175/JTECH-D-20-0005.1>
- Lang, T. J., Miller, L. J., Weisman, M., Rutledge, S. A., Barker, L. J., Bringi, V. N., et al. (2004). The severe thunderstorm electrification and precipitation study. *Bulletin of the American Meteorological Society*, *85*(8), 1107–1125. <https://doi.org/10.1175/BAMS-85-8-1107>
- Lang, T. J., & Rutledge, S. A. (2011). A framework for the statistical analysis of large radar and lightning datasets: Results from STEPS 2000. *Monthly Weather Review*, *139*(8), 2536–2551. <https://doi.org/10.1175/MWR-D-10-05000.1>
- Leal, A. F., Rakov, V. A., & Rocha, B. R. (2019). Compact intracloud discharges: New classification of field waveforms and identification by lightning locating systems. *Electric Power Systems Research*, *173*, 251–262. <https://doi.org/10.1016/j.epsr.2019.04.016>
- Li, Y., Zhang, G., & Zhang, Y. (2020). Evolution of the charge structure and lightning discharge characteristics of a Qinghai-Tibet plateau thunderstorm dominated by negative cloud-to-ground flashes. *Journal of Geophysical Research: Atmospheres*, *125*(5). <https://doi.org/10.1029/2019JD031129>
- López, J. A., Montanyà, J., van der Velde, O. A., Pineda, N., Salvador, A., Romero, D., et al. (2019). Charge structure of two tropical thunderstorms in Colombia. *Journal of Geophysical Research: Atmospheres*, *124*(10), 5503–5515. <https://doi.org/10.1029/2018JD029188>
- Ma, Z., Jiang, R., Qie, X., Xing, H., Liu, M., Sun, Z., et al. (2021). A low frequency 3D lightning mapping network in north China. *AtmRe*, *249*, 105314. <https://doi.org/10.1016/J.ATMOSRES.2020.105314>
- MacGorman, D. R., Burgess, D. W., Mazur, V., Rust, W. D., Taylor, W. L., & Johnson, B. C. (1989). Lightning rates relative to tornadic storm evolution on 22 May 1981. *Journal of the Atmospheric Sciences*, *46*(2), 221–251. [https://doi.org/10.1175/1520-0469\(1989\)046<0221:lrrrts>2.0.co;2](https://doi.org/10.1175/1520-0469(1989)046<0221:lrrrts>2.0.co;2)
- MacGorman, D. R., David Rust, W., Schuur, T. J., Biggerstaff, M. I., Straka, J. M., Ziegler, C. L., et al. (2008). TELEX the thunderstorm electrification and lightning experiment. *Bulletin of the American Meteorological Society*, *89*(7), 997–1013. <https://doi.org/10.1175/2007BAMS2352.1>
- MacGorman, D. R., & Rust, W. D. (1998). *The electrical nature of storms*. Oxford University Press.
- MacGorman, D. R., Rust, W. D., Krehbiel, P., Rison, W., Bruning, E., & Wiens, K. (2005). The electrical structure of two supercell storms during STEPS. *Monthly Weather Review*, *133*(9), 2583–2607. <https://doi.org/10.1175/MWR2994.1>
- Mansell, E. R., Ziegler, C. L., & Bruning, E. C. (2010). Simulated electrification of a small thunderstorm with two-moment bulk microphysics. *Journal of the Atmospheric Sciences*, *67*(1), 171–194. <https://doi.org/10.1175/2009JAS2965.1>
- Mazur, V., & Ruhnke, L. H. (1993). Common physical processes in natural and artificially triggered lightning. *Journal of Geophysical Research*, *98*(D7), 12913–12930. <https://doi.org/10.1029/93JD00626>
- Mecikalski, R. M., Bitzer, P. M., & Carey, L. D. (2017). Why flash type matters: A statistical analysis. *Geophysical Research Letters*, *44*(18), 9505–9512. <https://doi.org/10.1002/2017GL075003>
- Medina, B. L., Carey, L. D., Lang, T. J., Bitzer, P. M., Deierling, W., & Zhu, Y. (2021). Characterizing charge structure in central Argentina thunderstorms during RELAMPAGO utilizing a new charge layer polarity identification method. *Earth and Space Science*, *8*(8), e2021EA001803. <https://doi.org/10.1029/2021EA001803>
- Meyer, V. K., Höller, H., & Betz, H. D. (2013). Automated thunderstorm tracking: Utilization of three-dimensional lightning and radar data. *Atmospheric Chemistry and Physics*, *13*(10), 5137–5150. <https://doi.org/10.5194/acp-13-5137-2013>
- Murphy, M. J., Cramer, J. A., & Said, R. K. (2021). Recent history of upgrades to the U.S. National Lightning Detection Network. *Journal of Atmospheric and Oceanic Technology*, *38*(3), 573–585. <https://doi.org/10.1175/JTECH-D-19-0215.1>
- Orville, R. E. (2008). Development of the national lightning detection network. *Bulletin of the American Meteorological Society*, *89*(2), 180–190. <https://doi.org/10.1175/BAMS-89-2-180>
- Pawar, S. D., & Kamara, A. K. (2007). End-of-storm oscillation in tropical air mass thunderstorms. *Journal of Geophysical Research*, *112*(D3), 3204. <https://doi.org/10.1029/2005JD006997>
- Pawar, S. D., & Kamra, A. K. (2004). Evolution of lightning and the possible initiation/triggering of lightning discharges by the lower positive charge center in an isolated thundercloud in the tropics. *Journal of Geophysical Research*, *109*(D2), 2205. <https://doi.org/10.1029/2003JD003735>
- Pedeboy, S. (2015). Analysis of the French lightning locating system location accuracy. 2015 International Symposium on Lightning Protection. *XIII SIPDA*, 337–341. <https://doi.org/10.1109/SIPDA.2015.7339299>
- Pédeboy, S., Barnéoud, P., Defer, E., & Coquillat, S. (2018). Analysis of the intra-cloud lightning activity detected with low frequency lightning locating systems. In *25th International Lightning Detection Conference*.
- Pedregosa, F., Michel, V., Grisel, O., Blondel, M., Prettenhofer, P., Weiss, R., et al. (2011). Scikit-learn: Machine learning in Python. *Gaël Varoquaux Bertrand Thirion Vincent Dubourg Alexandre passos PEDREGOSA, VAROQUAUX, GRAMFORT ET AL. Matthieu perrot. Journal of Machine Learning Research*, *12*, 2825–2830.
- Pereyra, R. G., Avila, E. E., Castellano, N. E., & Saunders, C. P. (2000). A laboratory study of graupel charging. *Journal of Geophysical Research*, *105*(D16), 20803–20812. <https://doi.org/10.1029/2000JD900244>
- Pineda, N., Rigo, T., Montanyà, J., & van der Velde, O. A. (2016). Charge structure analysis of a severe hailstorm with predominantly positive cloud-to-ground lightning. *Atmospheric Research*, *178–179*, 31–44. <https://doi.org/10.1016/J.ATMOSRES.2016.03.010>
- Qie, X., Zhang, T., Chen, C., Zhang, G., Zhang, T., & Wei, W. (2005). The lower positive charge center and its effect on lightning discharges on the Tibetan Plateau. *Geophysical Research Letters*, *32*(5), 1–4. <https://doi.org/10.1029/2004GL022162>
- Ribaud, J. F., Bousquet, O., & Coquillat, S. (2016). Relationships between total lightning activity, microphysics and kinematics during the 24 September 2012 HyMeX bow-echo system. *Quarterly Journal of the Royal Meteorological Society*, *142*, 298–309. <https://doi.org/10.1002/qj.2756>
- Rison, W., Thomas, R. J., Krehbiel, P. R., Hamlin, T., & Harlin, J. (1999). A GPS-based three-dimensional lightning mapping system: Initial observations in central New Mexico. *Geophysical Research Letters*, *26*(23), 3573–3576. <https://doi.org/10.1029/1999GL010856>
- Rust, W. D., MacGorman, D. R., Bruning, E. C., Weiss, S. A., Krehbiel, P. R., Thomas, R. J., et al. (2005). Inverted-polarity electrical structures in thunderstorms in the severe thunderstorm electrification and precipitation study (STEPS). *Atmospheric Research*, *76*(1–4), 247–271. <https://doi.org/10.1016/J.ATMOSRES.2004.11.029>
- Rutledge, S. A., Hilburn, K. A., Clayton, A., Fuchs, B., & Miller, S. D. (2020). Evaluating geostationary lightning mapper flash rates within intense convective storms. *Journal of Geophysical Research: Atmospheres*, *125*(14), e2020JD032827. <https://doi.org/10.1029/2020JD032827>
- Salvador, A., Pineda, N., Montanyà, J., López, J. A., & Solà, G. (2021). Thunderstorm charge structures favouring cloud-to-ground lightning. *Atmospheric Research*, *257*, 105577. <https://doi.org/10.1016/j.atmosres.2021.105577>

- Saunders, C. P., Keith, W. D., & Mitzeva, R. P. (1991). The effect of liquid water on thunderstorm charging. *Journal of Geophysical Research*, 96(D6), 11007–11017. <https://doi.org/10.1029/91JD00970>
- Saunders, C. P., & Peck, S. L. (1998). Laboratory studies of the influence of the rime accretion rate on charge transfer during crystal/graupel collisions. *Journal of Geophysical Research*, 103(D12), 13949–13956. <https://doi.org/10.1029/97JD02644>
- Schultz, C. J., Carey, L. D., Schultz, E. V., & Blakeslee, R. J. (2015). Insight into the kinematic and microphysical processes that control lightning jumps. *Weather and Forecasting*, 30(6), 1591–1621. <https://doi.org/10.1175/WAF-D-14-00147.1>
- Schultz, C. J., Petersen, W. A., & Carey, L. D. (2009). Preliminary development and evaluation of lightning jump algorithms for the real-time detection of severe weather. *Journal of Applied Meteorology and Climatology*, 48(12), 2543–2563. <https://doi.org/10.1175/2009JAMC2237.1>
- Schulz, W., Diendorfer, G., Pedeboy, S., & Roel Poelman, D. (2016). The European lightning location system EUCLID—Part 1: Performance analysis and validation. *Natural Hazards and Earth System Sciences*, 16(2), 595–605. <https://doi.org/10.5194/NHESS-16-595-2016>
- Stolzenburg, M., Rust, W. D., & Marshall, T. C. (1998). Electrical structure in thunderstorm convective regions: 3. Synthesis. *Journal of Geophysical Research*, 103(D12), 14097–14108. <https://doi.org/10.1029/97JD03545>
- Stough, S. M., & Carey, L. D. (2020). Observations of anomalous charge structures in supercell thunderstorms in the Southeastern United States. *Journal of Geophysical Research: Atmospheres*, 125(17), e2020JD033012. <https://doi.org/10.1029/2020JD033012>
- Stough, S. M., Carey, L. D., Schultz, C. J., & Cecil, D. J. (2021). Examining conditions supporting the development of anomalous charge structures in supercell thunderstorms in the Southeastern United States. *Journal of Geophysical Research: Atmospheres*, 126(16), e2021JD034582. <https://doi.org/10.1029/2021JD034582>
- Takahashi, T. (1978). Riming electrification as a charge Generation mechanism in thunderstorms in: Journal of the atmospheric Sciences Volume 35 Issue 8. *Journal of the Atmospheric Sciences*, 35, 1536–1548. [https://doi.org/10.1175/1520-0469\(1978\)035<1536:reaacg>2.0.co;2](https://doi.org/10.1175/1520-0469(1978)035<1536:reaacg>2.0.co;2)
- Tessendorf, S. A., Rutledge, S. A., & Wiens, K. C. (2007). Radar and lightning observations of normal and inverted polarity multicellular storms from STEPS. *Monthly Weather Review*, 135(11), 3682–3706. <https://doi.org/10.1175/2007MWR1954.1>
- Thomas, R. J., Krehbiel, P. R., Rison, W., Hunyady, S. J., Winn, W. P., Hamlin, T., & Harlin, J. (2004). Accuracy of the lightning mapping array. *Journal of Geophysical Research*, 109(D14), 14207. <https://doi.org/10.1029/2004JD004549>
- Van Der Velde, O. A., & Montanyà, J. (2013). Asymmetries in bidirectional leader development of lightning flashes. *Journal of Geophysical Research: Atmospheres*, 118(24), 13504–13519. <https://doi.org/10.1002/2013JD020257>
- Weiss, S. A., Macgorman, D. R., & Calhoun, K. M. (2012). Lightning in the Anvils of supercell thunderstorms. *Monthly Weather Review*, 140(7), 2064–2079. <https://doi.org/10.1175/MWR-D-11-00312.1>
- Wiens, K. C., Rutledge, S. A., & Tessendorf, S. A. (2005). The 29 June 2000 supercell observed during STEPS. Part II: Lightning and charge structure. *Journal of the Atmospheric Sciences*, 62(12), 4151–4177. <https://doi.org/10.1175/JAS3615.1>
- Williams, E., Mushtak, V., Rosenfeld, D., Goodman, S., & Boccippio, D. (2005). Thermodynamic conditions favorable to superlative thunderstorm updraft, mixed phase microphysics and lightning flash rate. *Atmospheric Research*, 76(1–4), 288–306. <https://doi.org/10.1016/j.ATMOSRES.2004.11.009>
- Williams, E. R. (1985). Large-scale charge separation in thunderclouds. *Journal of Geophysical Research*, 90(D4), 6013–6025. <https://doi.org/10.1029/JD090ID04P06013>
- Williams, E. R. (1989). The tripole structure of thunderstorms. *Journal of Geophysical Research*, 94(D11), 13151–13167. <https://doi.org/10.1029/JD094ID11P13151>